SSRG International Journal of Electrical and Electronics Engineering
ISSN: 2348-8379/ https://doi.org/10.14445/23488379/IJEEE-V11I7P107

Volume 11 Issue 7, 78-101, July 2024

Original Article

A Novel Hybridized Optimization Mechanism for Efficient Channel Estimation Using Adaptive and Attention-Based Convolutional Autoencoder in MIMO-NOMA for mmWave Systems

Belcy D. Mathews[1], Tamilarasi Muthu[2]

[1,2]*Department of Electronics and Communication Engineering, Puducherry Technological University, Puducherry, India.*

[1]*Corresponding Author : mathews.d.belcy@gmail.com*

Received: 03 May 2024 Revised: 06 June 2024 Accepted: 04 July 2024 Published: 26 July 2024

Abstract *- The channel estimation is crucial in the "millimeter Wave (mmWave) Massive Multiple-Input Multiple-Output (MIMO) and Non-Orthogonal Multiple Access (NOMA)" devices. Hybrid beamforming techniques are employed nowadays to minimize the complexity and equipment price. However, the absence of digital beam forming in mmWave affects the dynamic range and accuracy of the channel estimation. Previous research is concentrated mainly on predicting narrow-band mmWave channels using deep learning networks as the wideband channels of mmWave create a considerable amount of range and noise issues. Accurate channel estimation in the MIMO system is challenging because of the increased number of antennas and Radio-Frequency (RF) chains. MIMO system communications using mmWave are frequently chosen because of their massive spectrum resources. Therefore, it is essential to tackle the obstacles obtained in the standard channel estimation framework by developing a MIMO-NOMA network with the help of deep learning methods. In this paper, an advanced tuning and prediction approach with a deep learning mechanism is designed to perform an accurate estimation of channels for the MIMO-NOMA system. Moreover, a hybridized optimization model called Wild Horse-Piranha Foraging Optimization Algorithm (WH-PFOA) is developed and utilized with Adaptive and Attention-based Convolutional Autoencoder (Ada-ACAE) for estimating the channels in mmWave-based MIMO-NOMA system. Furthermore, the complexity rate and the hardware cost of the MIMO-NOMA network are reduced by adapting the hybrid beam-forming mechanism. Initially, to perform channel estimation, the pilot symbols are tuned by the introduced WH-PFOA to enhance the channel estimation performance. Later, the channel estimation is carried out with the optimal pilot symbols and the channel coefficients are validated. Numerical results show that the proposed channel estimation and pilot estimation process outperforms the state-of-the-art approaches.*

Keywords *- Millimeter wave network, Massive Multiple-Input Multiple-Output, Non-Orthogonal Multiple Access, Attention-based convolutional autoencoder, Wild horse-piranha foraging optimization algorithm.*

1. Introduction

MmWave MIMO and NOMA wireless communication is a significant innovation for the Sixth Generation (6G) wireless communications since they are capable of creating novel resources for spectrum and substantially raising the rate of wireless transmission [1]. However, the mmWave is associated with the high frequency band and transmits on the vacuum like a direct wave having a narrow beam and noticeable absorption features. Therefore, path loss on mmWave becomes considerably greater than that in the low-frequency band [2]. Through the utilization of a huge antenna array, visibility is boosted, and power is focused on the receiving device. Additionally, the expanded mmWave's bandwidth boosts the system needs for the Analog-to-Digital Converter (ADC). Hence, during execution, building a receiving framework by combining a high-resolution ADC and a huge antenna array is too complex and they are highly expensive [3]. At present, the relevant research comprises two major options. The initial step is to employ a combined precoding framework [4]. An analog beam former can minimize the ADCs and RF chains count on the framework, which results in balancing the hardware expense [5]. Another option is the choice to employ low-resolution ADCs rather than high-resolution ADCs, which immediately minimizes the system's power consumption and hardware expenses, although quantization noise remains an inevitable concern [6].

The estimation of channels has become an important topic in the area of mmWave interactions, and various channel

estimation approaches have been established over the recent time span [7]. Channel estimation strategies for mmWave devices are divided into two categories of beamforming frameworks, namely completely digital beamforming frameworks with poor resolution and hybrid beamforming frameworks with an optimal state (high-resolution) ADC for quantization [8]. In a complete digital beamforming framework, every antenna on the network is supplied with a related RF chain that enables the adaptable and effective creation of several adaptable beams, but the antenna count is frequently restricted because of hardware expenses [9]. The combined beamforming framework is comprised of two components, namely a "low-dimensional digital beamforming system with lesser RF chains and an analog beamforming system with an analog phase shifter" that is employed in situations with more antennas and resolves the issue of increased loss of data transfer on the mm bands [10]. Additionally, by assuming the effect of quantization noise during data transfer of signals while employing a low-resolution ADC, the researchers suggested a mixed-ADC system [11]. This combined structure is cost-effective since it substantially decreases the cost of hardware and power consumption throughout this duration period [12].

Currently, mixed-ADC structure connected with mmWave massive MIMO is becoming a mainstream of communication, successfully tackling the problem of increased power usage as well as the expense related to Base Station (BS) circuits [13]. However, the issue raised due to channel estimation on mmWave massive MIMO framework using mixed-ADC structure remains to be examined [14]. Currently, the "Intelligent Reflective Surface (IRS)" has generated major interest in communications [15]. For the IRS-aided communication channel estimation issue, the investigators suggested a cell on/off state control-aided channel estimation method that is capable of estimating the client's reflected channel by avoiding interference caused by other IRS components' transmitted signals [16]. Still, installing a significant amount of on/off switches is expensive since every IRS component should be separately controlled [17]. Assuming the network overhead issue, we developed a channel estimation approach.

The key objectives of the introduced channel estimation model for MIM0-NOMA systems are discussed below.

- To suggest an advanced and improved channel estimation framework for the mmWave networks to attain increased information rate, reliability, and efficiency through the usage of deep learning techniques.
- To implement an advanced deep learning model named Ada-ACAE by integrating an attention module to the CAE framework to perform channel estimation. ACAE-aided channel estimation allows the framework to record the temporal and spatial dependencies of the network and promotes exact estimation.
- To generate an advanced tuning approach by embedding traditional WHO and PFOA strategy to attain the optimal pilot design and also to tune the parameters of the Ada-ACAE framework to minimize BER and MSE.
- To explore the efficacy of the introduced channel estimation mechanism via classic meta-heuristic strategies.

The effective channel estimation scheme implemented is explained below. The merits and demerits of the traditional channel estimation networks are presented in Part 2. An overview of the channel estimation in MIMO-NOMA for the mmWave framework is discussed in Part 3. Part 4 provides a brief description of the implemented wild horse-piranha foraging optimization algorithm-aided hybrid beamforming for the channel estimation model. Part 5 deals with the implemented channel estimation model using adaptive and attention-based deep learning mechanisms. Part 6 conveys the results achieved by the implemented channel estimation network, and the conclusions of the suggested model are laid out in Part 7.

2. Literature Survey

2.1. Related Works

Zhang et al. [18] have generated a novel "repetitive reweight based log-sum constraint channel estimation approach". Employing log-sum as a constraint by tuning an objective via the technique of gradient descent approach, the suggested approach will repeatedly shift the channel estimated "Angle-of-Departures (AODs) and Angle-of-Arrivals (AOAs)" and to the best possible outcomes substantially enhancing angle estimation efficiency. Additionally, in order to ensure channel estimate efficiency, an adaptive regularization element was developed to utilize channel estimation sparsity and information fitting error. Experimental results demonstrated that the recommended method has superior convergence than traditional approaches.

In 2019, Kim and Choi [19] developed a "Fully Corrective Forward Greedy Selection-Cross Validation (FCFGS-CV)-based channel estimation approach" for multichannel mmWave-massive MIMO networks employing "low-resolution Analog-to-Digital Converters (ADCs)". The sparse characteristic of the mmWave simulated channels in the delay and angular domains was employed to modify the "Maximum A Posteriori (MAP)" based estimation issue to a tuning issue via a sparsity constraint and concave objective function.

The sparsity-constrained tuning problem had been resolved using the FCFGS algorithm, formerly referred to as the generalized "Orthogonal Matching Pursuit (OMP)" approach. Moreover, this technique was employed to predict the accurate situation of termination by determining the overfitting while the sparsity level was undefined.

In 2023, Zhang et al. [20] have initiated a sparse channel estimation method. Particularly, considering the usage of the sparsity on the mmWave channels, beam space-based channel estimation issues were converted into a sparse matrix recovery issue, along with the parameters of the channel improved by employing the Compressive Sensing (CS) approach. Experimental outcomes have demonstrated that this approach quantized via combined ADC exceeded the low-resolution ADC. If the "low-resolution ADC" in the combined ADC design attains five bits, the maximized performance was attained.

In 2023, Ahmad and Young [21] recommended a mMIMO-NOMA network-based detection and channel estimation techniques that employ a deep learning approach to manage the problem due to incorrect signal recognition attained because of inaccurate user interference, channel noise and Channel State Information (CSI). Experimental analysis demonstrated that the introduced approach shows superior performance.

In 2022, Chen et al. [22] introduced a "compressive channel estimation approach for IRS-assisted mmWave Multi-Input/Multi-Output (MIMO) network". Employing Kronecker product features, the IRS-aided mmWave channel was transformed into a sparse signal detection issue comprising two opposing terms of the cost function. Traditional sparse recovery approaches tackled the integrated contradicting objectives by employing a regularization parameter, resulting in a suboptimal outcome. Experimental examination demonstrated that under a huge variety of simulation parameters, the suggested approach exhibited competitive error efficiency compared to the existing channel estimating approach.

In 2018, He et al. [23] generated a "Learned Denoising-aided Approximate Message Passing (LDAMP) system". This neural framework can investigate channel topology and estimate the channel using a vast amount of training information. Moreover, the created network offered an analytical network for evaluating the channel estimator's asymptotic efficiency. According to the simulation outcome, this network greatly exceeded traditional methods of compressed sensing-aided models even when the receiver has a smaller amount of RF chains.

In 2022, Abdallah et al. [24] introduced a "frequency-selective broadband mmWave model and developed two deep learning Compressive Sensing methods" for channel estimation. The developed strategy attains essential data from training data, resulting in extremely exact channel estimations with minimal expenses. The initial technique employed a deep learning and CS-aided strategy to estimate channels in the frequency domain that were subsequently employed to reconstruct the channel. Experimental analysis demonstrated that the proposed model outperformed the conventional Orthogonal Matching Pursuit (OMP) approach based on computational complexity, spectral efficiency, and NMSE.

In 2021, Ma et al. [25] proposed a "Model-Driven Deep Learning (MDDL)-aided channel estimate and feedback strategy for broadband mmWave large hybrid MIMO network" for leveraging the scantness of angle-delay domain channels to reduce network overhead. Particularly through exploiting the structured scantiness of the channel from an existing network, learning the embedded trainable features from the sample information and developing the "Multiple-Measurement-Vectors Learned Approximate Message Passing (MMV-LAMP) model".

2.2. Problem Statement

Channel estimation in the MIMO-NOMA generates complicated issues when the receivers are provided with maximal counts of RF chains in the mmWave massive MIMO system. Furthermore, it is complicated to develop receiver architecture with higher-resolution ADC and antenna arrays in practical communication applications because they are expensive. Advancements and complications related to the ordinary channel estimation schemes in the MIMO-NOMA for the mmWave model are tabulated in Table 1.

The gradient descent technique [18] utilizes the flexible regularization parameters to modify the trade-off among the data filling errors and sparse weighted sums. However, selecting the learning is a complicated task and it is subjected to overfitting. FCFGS-CV and OMP [19] provide more accurate outcomes in a limited time period, and their implementation procedures are simple. Yet, it needs to rectify the time complexity issues in the encoder region. Mixed ADC [20] attains minimal estimation errors than the existing mechanism, while enormous frames are utilized. However, it did not provide better outcomes in the cascaded channel generation phase.

DWT [21] effectively minimizes the noise rate and inter-channel interference rate in the system, and it also has a good localization rate in the spatial frequency domain. However, it needs to tackle the shift variance issues, and it is also complicated to understand the implementation procedures. Hybrid evolutionary theory [22] minimizes the overhead issues when training is executed in the system. Yet, it requires effectual improvement in the receiver.

Neural networks and LDAMP [23] easily study the structure of the channel and validate the channel from enormous training data and also it accurately provides the effectualness rate in minimal time. Yet, it needs to overcome the overfitting issues, and also it requires enormous labeled training data for the validations.

OMP [24] offers a more precise channel estimation rate along with minimal training overheads. However, it needs to

enhance the spectral efficiency rate and also its implementation is expensive. MMV-LAMP [25] effectively resolves the uplink overhead issues to perform high-dimensional channel estimation in the RF chains. Yet, it needs to minimize the overhead issues in the model. Hence, it is essential to develop an efficient channel estimation framework in the MIMO-NOMA structure by looking into the limitations of the existing techniques.

3. Channel Estimation in MIMO-NOMA for mmWave Systems: Overview

3.1. MIMO Channel Model

Assume a massive MIMO network that uses a BS combined with RF chains B_r^{Rf} and antennas B_r to transfer the signals to one user equipped with RF chains B_e^{Rf} and antennas B_e. The phase shifters are utilized for connecting an enormous amount of antennas with considerably less number of RF chains from the consumer side and BS. Therefore, consider $B_r >> B_r^{Rf}$ and $B_e >> B_e^{Rf}$. The B_e x B_r channel matrices among the recipient and the sender at the delay domain are presented in Equation (1).

$$G(\tau) = \sum_{K=1}^{K} \alpha_k \delta(\tau - \tau_k) L_E(\varphi_k) L \frac{G}{R}(\phi_k) \qquad (1)$$

Here, the term K represents the total amount of primary paths, the term $\alpha_k \approx XB(0,\sigma_\alpha^2)$ indicates the transmission gain for k^{th} channel with σ_α^2 indicating the mean power gain, the term τ_k denotes the delay on k^{th} route, and the terms φ and $\phi \epsilon [0,2\pi]$ are the azimuth angles of both departure and arrival (AoA/AoD) on the receiving end and transmitting device, correspondingly. The reaction matrices of a Uniform Linear Array (ULA) and presented below.

$$L_E(\varphi) = \frac{1}{\sqrt{B_e}} \left[1, w^{-k2\pi \frac{s}{\lambda} \sin\varphi_k}, \ldots, w^{-k2\pi \frac{s}{\lambda}(B_e - 1)\sin\varphi_k} \right]^R \qquad (2)$$

$$L_R(\phi) = \frac{1}{\sqrt{B_e}} \left[1, w^{-k2\pi \frac{s}{\lambda} \sin\phi_k}, \ldots, w^{-k2\pi \frac{s}{\lambda}(B_r - 1)\sin\phi_k} \right]^R \qquad (3)$$

Here, the distance separating the neighboring carrier wavelength and antennas are denoted by the terms λ and s correspondingly.

3.2. NOMA Model

During Power Domain (PD) NOMA, multiple clients utilize an identical orthogonal energy unit yet show varying power ratings. Customers with enhanced channel settings receive less power, and inversely. Figure 1 depicts the NOMA technique using a power domain multiplexer.

Assume the situation of two individuals, namely User 1 and User 2. Consider a User 1 employs an effective channel when compared with User 2, i.e.,$|g_1| > |h_2|$ As an outcome, User 1 gets a low power supply, whereas User 2 obtains a higher one. In the receiver end, User 2 immediately decodes the incoming signal by considering the User 1 signal as sound. Yet, in User 1, immediate identification cannot be feasible because the greater power supply is assigned to User 2, leading to substantial interference by User 2. As an outcome, User 1 initially identifies and decodes User 2's signals before deleting them via Successive Interference Cancellation (SIC). Following SIC, User 1 recognizes their signal from noise. This approach demands CSI to be known by both the BS and the user. The basic NOMA network is presented in Figure 1.

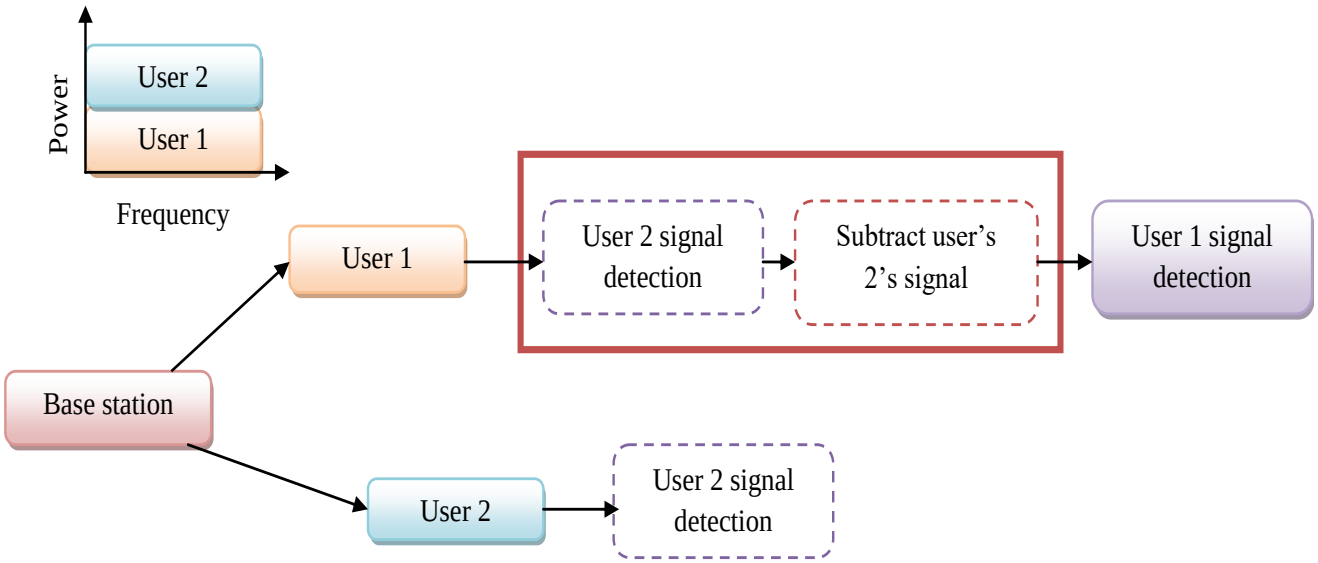

Fig. 1 Pictorial representation of the basis of the NOMA model

3.3. System Model: Overview

In this proposed channel estimation scheme, the input information is fed to a converter, where a serial stream of the input information is transformed into parallel data. Later, the attained parallel data is offered to the 64-QAM block that employs a single radio wave in order to denote the six bits of the attained parallel data. A modulator is linked with a subcarrier block to create the pilot blocks. Here, the signals are changed to the time domain by utilizing the "Inverse Fast Fourier Transform (IFFT)" technique. Further, Cyclic Prefix (CP) is also embedded in conflict multipath fading, where the length of the multipath fading exceeds the highest delay speed of the channel. An introduced WH-PFOA strategy is employed to tune the pilot symbol to attain the optimal pilot symbol. The attained optimal pilot symbol helps to enhance the channel estimation efficiency. Channel estimation is performed on the introduced Ada-ACAE framework by considering the CSI matrix as the input. The key objective of the channel estimation is to reduce the error rate in the MIMONOMA framework by tuning the network parameters using WH-PFOA. The block diagram of the developed Ada-ACAE-based channel estimation framework is in Figure 2.

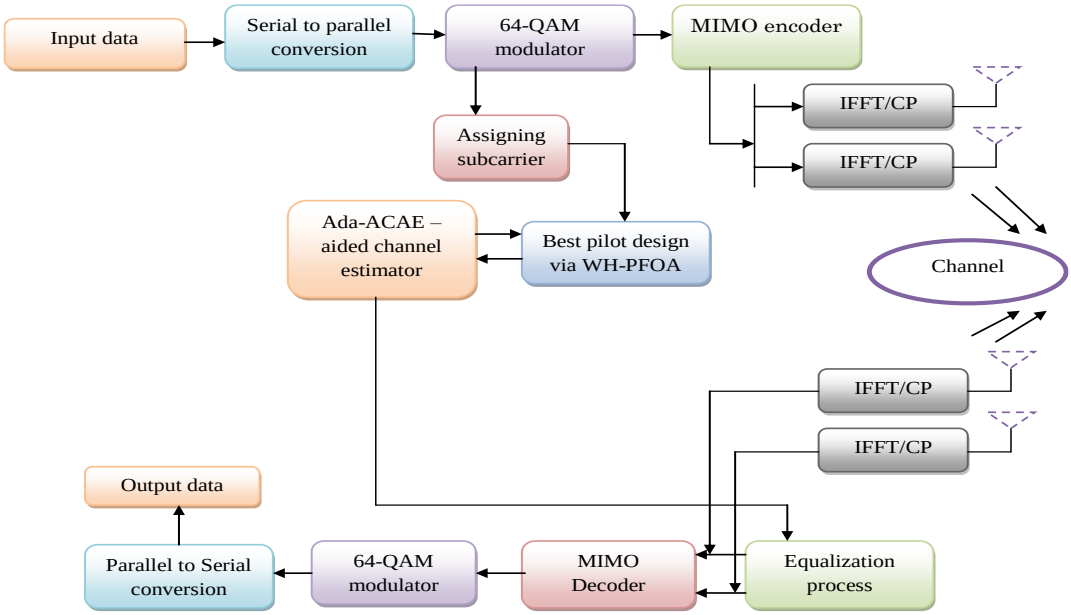

Fig. 2 Block diagram of the Ada-ACAE-based channel estimation framework

4. Wild Horse-Piranha Foraging Optimization Algorithm-Based Hybrid Beamforming for Channel Estimation Model

4.1. Hybrid Beamforming Model

Let us assume a MIMO-NOMA in a macro cell of radii 500m. BS offers the transmit power O_{va} and equivalently splits it between the antenna B. Thus, the BS sends the superimposed signal on the basis of NOMA features. Every UE N is arbitrarily given to the cells to generate MIMO-NOMA conditions. Here, the power transmitted via a single antenna is denoted as $o_b=O_{va}/B$. In the MIMO-NOMA model, the UE near the BS employs a SIC approach to eliminate the interference signals. Additionally, the BS is liable to perform clustering of the UE and also to identify the transmit power of the UE. "Additive White Gaussian Noise (AWGN)" and Rayleigh fading have an impact on the signals attained on every UE. The signal transferred by the BS is expressed in Equation (4).

$$z_b = \Sigma_{j=1}^{J} \sqrt{\alpha_{b,j}} O_b a_{b,j} \tag{4}$$

Here, the terms O_b, $\alpha_{b,j}$, and $a_{b,j}$ represent the power transmitted on every beam with J users, power allocation coefficient and transferred signals. The signals attained by $UE_{b,j}$,

$$t_{b,j} = g_{b,j} \Sigma_{b=1}^{B} q_b z_h + b_{b,j} \tag{5}$$

Here, the term $g_{b,j}$ denotes the Rayleigh fading channel vector, which is evaluated between BS to $UE_{b,j}$, the term q_b indicates the precoding vector and the term $Q=[q_1, q_2,\ldots.q_b]$ here $q_b \epsilon X^{1xB}$, and the term $b_{b,j}$ denotes the AWGN, and the term $g_{b,j}$ is numerically defined in Equation (6).

$$g_{b,j} = a_{b,j} \sqrt{s_{b,j}^{-\delta}} \tag{6}$$

Here, the term $s_{b,j}$ denotes the division between BS and $UE_{b,j}$ variable δ. The power allocation coefficient $\alpha_{b,j}$ based on the NOMA principles is presented in Equation (7).

$$0 \geq \alpha_{b,j} \leq 1, \ \Sigma_{j=1}^{J} \alpha_{b,j} = 1, \ \alpha_{b,j} \in \forall \tag{7}$$

Here, the term $\forall$ represents the group of feasible power allocation coefficients. The receiver end consists of B number of isotropic antenna components that are divided into K subsets of the antenna array, where each subset has N number of antenna components.

RF chain count, B_{rf} is considered fewer than the antenna component's count on the hybrid beam foaming. Every antenna array component is lined in a single RF chain as a substitute for the antenna components. The hybrid beam forming network receives a desired signal $d_a(r)w^{h2\pi dxr}$ with Θ_j as the Angle of Arrival (AOA) and j number of interference signals $u_j(r)w^{h2\pi dxr}$ with a varying AOA Θ_k, where j=1,2,3,…,J. The attained signal $z_n(r)$ of the sub-array k in every n^{th} antenna component comprises an AWGN signal c(r), desired narrow signal band, and interference signal. Thus, the outcome attained at k^{th} sub-array $z_k(r)$ is presented in Equation (8).

$$z_k(r) = \Sigma_{n=0}^{N-1} d_a(r) w^{h2\pi dxr\left(r-\left(\frac{\sin\theta_s}{2\pi dx}\right).\tau_s\right)} + \Sigma_{n=0}^{N-1} u_j(r) w^{h2\pi dxr\left(r-\left(\frac{\sin\theta_j}{2\pi dx}\right).\tau_j\right)} + c(r) \quad (8)$$

Here, the term s denotes the distance among the nearest antenna array component assumed as 0.5τ. The variables τ_j and τ_s define the propagation delay of j^{th} the interference signal and the desired signal, and the term x expresses the intensity of the light. On the basis of the calculated baseband signal on a matrix-vector notation, every subset is expressed in Equation (9).

$$z(b) = D_{Rf}^{G} La(b) - D_{Rf}^{G} c(b) \quad (9)$$

Here, the term D_{Rf}^{G} describes the matrix diagonal, the term La(b) denotes the input of the analog beamforming phase, and the term c(b) indicates the noise vector. While applying the digital beamforming vector to the digital beamforming phase, Equation (9) is modified, as shown in Equation (10).

$$y(b) = d_S^{G} D_{Rf}^{G} La(b) - d_S^{G} D_{Rf}^{G} c(b) \quad (10)$$

The phase and signal amplitude are differentiated by changing the digital beamforming vector d_S. Hybrid Beamforming is used in the model to enhance the spectral efficiency. The systematic form of the Hybrid beamforming model is presented in Figure 3.

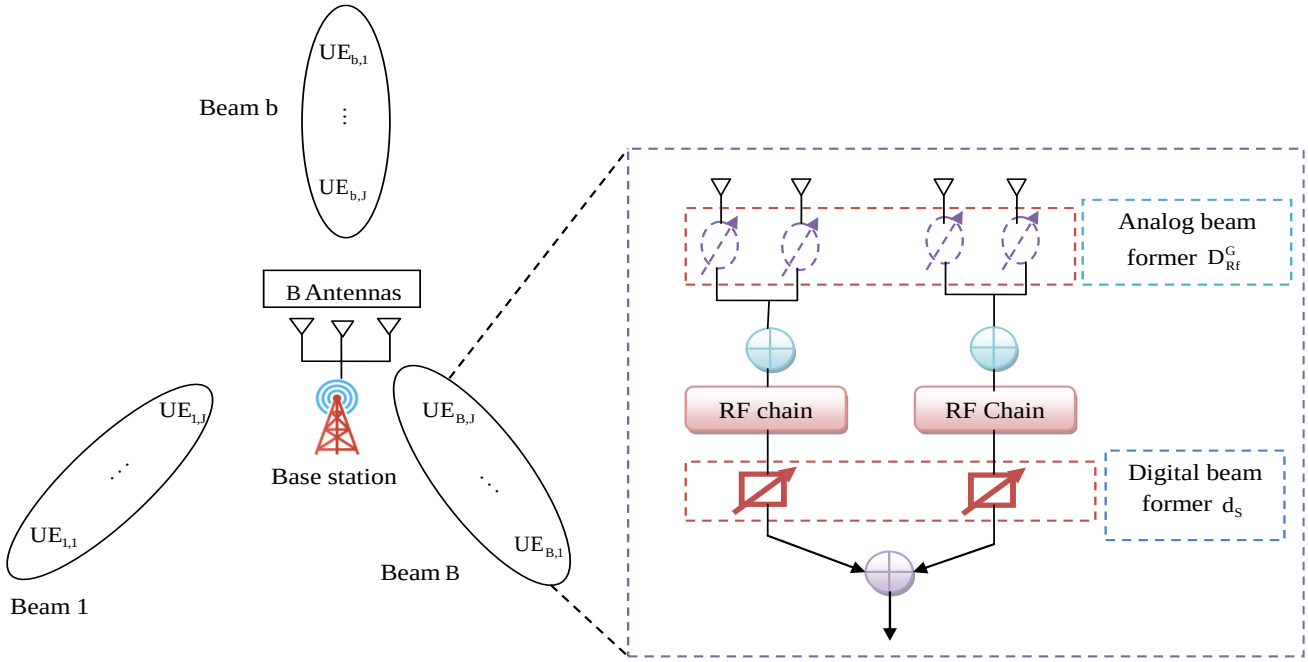

Fig. 3 Systematic form of the hybrid beamforming model

4.2. WH-PFOA for Optimal Pilot Design Tuning

WH-PFOA is developed by integrating the WHO and PFOA strategies, and WHO offers improved convergence efficiency. However, they face specific challenges due to the reduced exploitation capacity and stagnation in local optima. PHOA strategy prevents immature convergence and stagnation issues and offers effective performance within a short interval. However, they face difficulties in resolving high-dimensional tuning issues.

To tackle the issues faced by both algorithms, the WHO and PFOA are embedded and labeled as the WH-PFOA. They

possess the features of both WHO and PFOA strategies. In this introduced WH-PFOA, if (pc_{fit}>Md_{fit}), then the position is amended using WHO, or else the position is amended using PFOA. Here, the terms Pc_{fit} and Md_{fit} indicate the current fitness value and mean fitness value, respectively.

Optimization on Pilot Designs: The training symbols are also transferred with the information bits to guarantee pilot symbol-based channel estimation. Transferred vector z[j] is arranged in a matrix format and they are expressed as $Z \epsilon X^{BrxBe}$. In order to guarantee effective pilot-based channel estimation, a minimum number of B_r training symbols have to be transferred.

The matrix form of the training symbol is created by a set of orthogonal sequences that is subjected to $ZZ^r=\mu U_{BR}$, here; the term μ denotes the power of the signal related to the training symbol. The introduced WH-PFOA strategy is employed for tuning the pilot design to enhance the channel estimation performance.

In addition it also optimizes the parameters such as "activation function, count of hidden neurons, and epoch" in the Ada-ACAE framework for reducing the BER and MSE. The pseudo code of the introduced WH-PFOA is depicted in Algorithm 1.

Algorithm 1: WH-PFOA

```
Setup the parameters and population
While the criterion is not fulfilled
   For t=1 to maxtier
      For i=1 to Npop
         If (Pc_fit > Md_fit)
            The position is upgraded via the WHO
            Create an initial population
            Perform grazing behaviour
            Perform horse mating behaviour
            Select the group leadership
            Exchange and selection of leaders
         Else
         The position is upgraded via PFOA
           Initialize the position vector
           Define the predation intensity parameter
           Perform non-linear parametric control
           strategies
           Perform reverse escape search strategy
           Upgrade the proxy location formula
              Execute localized group attack pattern
              Execute bloodthirsty cluster attack pattern
              Execute scavenging foraging patterns
              Execute piranha population survival
              strategies
         End
      End
   End
End
```

The flowchart of the introduced WH-PFOA is presented in Figure 4.

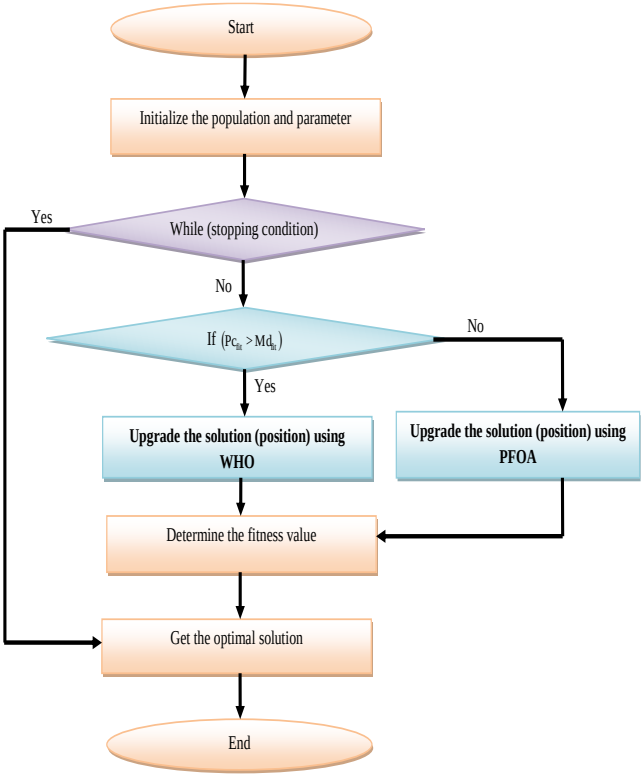

Fig. 4 Flowchart of WH-PFOA

4.3. Wild Horse Optimization Algorithm

The WHO [26] consists of five main steps and they are described below.

4.3.1. Creating an Initial Population

The fundamental model for all tuning approaches remains similar. This method begins with $(\bar{z}) = \{\bar{z}_1, z_2,\ldots..,\bar{z}_b\}$ a beginning arbitrary populace. The objective function examines this arbitrary populace continually, which generates an objective value of $(\bar{I}) = \{I_1, I_2,\ldots,I_b\}$.

In the beginning, the population of the horse is separated into various sets. If the total member's count in the population is denoted as B, then the group count is indicated as F=[BxOA]. Stallion's percentage OA on the entire population is assumed as the control parameter.

4.3.2. Grazing Behavior

The foals of the population generally graze near their group. The grazing behavior of the foal is numerically presented in Equation (11). This equation allows the members of the group to travel towards the leader and search nearby them at a distinct radius.

$$\vec{Z}^{h}_{u,,F} = 2M\cos(2\pi EM)\times\left(St^{h} - Z^{h}_{u,,F}\right) + St^{h} \qquad (11)$$

Here, the present location of the group member is denoted by the term Z_u^h, F, the location of the stallion is represented by the term St^h, the identical arbitrary integer within the interval [-2,2] is indicated by the term E, and the constant value Pi is denoted by the term π. The cos function attained by integrating π and E allow the horse to graze at various radius. The term indicates the latest location of the group member $\bar{z}_u^h$, F, and the adaptive mechanism evaluated via Equation (12) is represented by the term M.

$$\begin{aligned} &O = \vec{E}_1 < Tdr; \\ &Idx = (O == 0); \\ &M = E_2 \Theta Idx + \vec{E}_3 \Theta (\approx Idx) \end{aligned} \tag{12}$$

Here, the term O denotes the vector with the values 0 and 1 that is equivalent to the size of the issue; the term $\bar{E}_1$ and $\bar{E}_3$ indicates the arbitrary vectors within the interval [0, 1]. The term E_1 represents the arbitrary integer that lies between them [0, 1], and the term Idx indicates the indices of the arbitrary vector; the vector $\bar{E}_1$ fulfill the condition O==0, and the term Tdr denotes the adaptive parameter, which begins with the value 1 and gradually minimizes at the time of implementation and attains 0. It is arithmetically expressed in Equation (13).

$$Tdr = 1 - itr \times \left(\frac{1}{M_x itr} \right) \tag{13}$$

Here, the present iteration is denoted by the term itr, and the term represents the highest iteration count $M_x itr$.

4.3.3. Horse Mating Behavior

In order to imitate the mating and departure nature of the horses, a cross-over operator is developed. It is arithmetically presented in Equation (14).

$$\begin{aligned} &Z_{F,J}^{o} = Cs_{over}\left(Z_{F,u}^{p}, Z_{F,h}^{m}\right)\ u \neq h \neq j, o = p = end, \\ &Cs_{over} = Mn \end{aligned} \tag{14}$$

Here, the term $Z°_{F,J}$ indicates the location of the horse o from the set j, the term $Z^p_{F,u}$ indicates the location of the foal p from the set u, and the term $Z^m_{F,u}$ represents the horse m from the set h.

4.3.4. Group Leadership

The group's leaders have to direct the group to this water hole to utilize it if they are dominant; however, when another team is dominant, they have to move back. It is numerically presented in Equation (15).

$$\overline{St_{Fu}} = \begin{Bmatrix} 2M\cos(2\pi EM) \times (QG - St_{Fu}) + QG & \text{if } E_3 > 0.5 \\ 2M\cos(2\pi EM) \times (QG - St_{Fu}) - QG & \text{if } E_3 \leq 0.5 \end{Bmatrix} \tag{15}$$

Here, the term $\overline{St_{Fu}}$ indicates the next location of the leader from the set u, and the term QG denotes the location of the water hole, the term St_{Fu} denotes the present position of the leader from the set u, the term E expresses the identical arbitrary integer that lies within the interval [-2,2], and the term M represents the adaptive mechanism evaluated via Equation (11).

4.3.5. Exchange and Selection of Leaders

At first, the leader is chosen arbitrarily to protect the random nature of this approach. In the succeeding phases, the leaders are selected on the basis of their fitness rate. If the fitness of the group member is higher than the leader, then the leader and the member are exchanged. It is mathematically presented in Equation (16).

$$St_{Fu} = \begin{Bmatrix} Z_{F,u} & \text{if } \cos r(Z_{F,u}) < \cos r(St_{Fu}) \\ St_{Fu} & \text{if } \cos r(Z_{F,u}) > \cos r(St_{Fu}) \end{Bmatrix} \tag{16}$$

The pseudocode of WHO is given in Algorithm 2.

Algorithm 2: Conventional WHO

```
Setup the horse's initial population arbitrarily
Initialize the parameters
Compute the fitness function
Establish the foal set and choose the stallions
Determine the optimal horse
While the criterion is not fulfilled
   Evaluate Tdr via Equation (13)
   For stallion's count
      Compute M through Equation (12)
      For the number of foals in any group
         If rand > Pc
            Upgrade the foal's location via Equation (11)
         Else
            Upgrade the foal's location via Equation (14)
         End
      End
      If rand > 0.5
         Upgrade the location of St_Fu (bar) via Equation (15)
      Else
      Upgrade the location of St_Fu (bar) through Equation (15)
      End
      If cost(St_Fu (bar)) < cost(stallion)
         stallion = St_Fu (bar)
      End
      Arrange the foals group based on the cost
      Determine the foal with low cost
      If cost(foal) < cost(stallion)
         Interchange the location of foal and stallion via Equation (14)
```

```
        End
    End
Upgrade the best solution
End
```

4.4. Piranha Foraging Optimization Algorithm

PFOA [27] strategy describes the three different patterns. This approach includes several stages, such as population initialization, population evaluation, and parameter and agent upgrading.

4.4.1. Population Initialization

The location vector for every member of the piranha population is initialized based on according to Equation (17).

$$c_o = An_o + \beta 1 \times \left(In_o - An_o\right) \tag{17}$$

Here, the position of o^{th} member in the piranha candidate solution is denoted by the term c_o, and the upper and lower boundaries are represented by the terms An_o and In_o. An arbitrary integer within the range [0,1] is represented by the term β1.

4.4.2. The Predation Intensity Parameter G

The piranhas are highly responsive in blood detection. This feature is affected by the blood concentration G_o and the distance f_o. The piranhas will move towards the region with high blood concentrations, as shown in Equation (18). This characteristic is influenced by both the between the prey and the piranha. It is numerically expressed in Equation (18).

$$\begin{aligned} G_o &= \beta 2 \times \frac{M_o}{4\pi f_o^2} \\ f_o &= c_{py} - c_u \\ M_o &= \left[c_o(r) - c_{o+1}(r)\right]^2 \end{aligned} \tag{18}$$

Here, the term G_o denotes the parameter of predation intensity for o^{th} individual piranha, the term f_o indicates the distance between o^{th} piranha and the food, the term M indicates the intensity's source, the term M_o denotes the source intensity perceived by o^{th} search agent, and the term β2 denotes an arbitrary integer within the range [0,1].

4.4.3. Non-Linear Parametric Control Strategies

Nonlinear parametric control methods serve as helpful methods to manage time-varying random mechanisms and to avoid early population convergence while also preserving silky and smooth transitions between exploration and exploitation. At the beginning and mid phases, greater values D enable the search agent to execute an "auditory-based global search and prevent them from being trapped into local optimal", but in the subsequent phases, PFOA could converge rapidly as D modifications, see Equation (19).

$$D = V \cdot \cos\left[\frac{\pi}{2} \otimes \left(\frac{r}{M_x itr}\right)\right]^4 \tag{19}$$

Here, the term $M_x$itr denotes the highest iteration count, and the variable V denotes the constant value; the term ⊗ denotes the product of the variable and value.

4.4.4. Reverse Escape Search Strategy

The reverse escaping search approach aims to employ a flag R to modify the path of the population's search, preventing the candidate populace from getting stuck in the local region and diverting searching to an alternate location to enhance the solution. It occurs continually during the search procedure, offering the search agent further chances to precisely and strictly examine the search region, see Equation (20).

$$R = \begin{cases} 1 & \beta 3 \le 0.5 \\ -1 & \beta 3 > 0.5 \end{cases} \tag{20}$$

Here, the term β3 represents an arbitrary integer that lies between [0,1].

4.4.5. Update the Proxy Location Formula

The Localized Group Attack Pattern

Piranha attacks the prey that is near them. It is mathematically expressed via Equation (21).

$$c_o(y+1) = \gamma 1 \sum_{l=1}^{qv} \frac{A_l(y) - c_o(y)}{qv} - c_{py}(y) \tag{21}$$

Here, the term $c_o(y+1)$ indicates the search agent's latest position, the term qv expresses a value that is created arbitrarily, and the term $A_1(y)$ represents the fraction of local population attacks, A∈C and the term C denotes the arbitrarily generated piranha's count. The term $c_o(y)$ denotes the present agent's location, the term $c_{py}(y)$ denotes the best agent's position determined in the prior repetition, and the term γ1 is a random number uniformly distributed [-2,2].

The Bloodthirsty Cluster Attack Pattern

The piranha is capable of scene the presence of prey through the smell of blood. If the concentration of the blood is high, they travel rapidly. Modifying the direction of motion, they can determine the position of the prey as in Equation (22).

$$\begin{aligned} c_o(y+1) = {} & \gamma 1 * r^{\gamma 2} * c_{py}(y) + \\ & H * c_{py}(y) * R * G_o + R * \beta_4 * D * G_o \end{aligned} \tag{22}$$

Here, the term γ2 denotes the arbitrary integer lies between the range [-1/2,1/2] and the term β4 denotes an arbitrary integer within the range [0,1]. The term H indicates the coefficient of the foraging ability of piranhas.

The Scavenging Foraging Patterns

Due to poor eyesight, they split the group and feed on seeds and carrion, as shown in Equation (23).

$$c_o(y+1) = \frac{1}{2}\left[r^{\gamma 2} * c_{V1}(y) - R * c_0(y)\right] \quad (23)$$

Here, the term R is a variable that updates the direction of movement, the term $c_{v1}(y)$ denotes the $V1^{th}$ agent location arbitrarily determined from the piranhas, $c_0(t)$ denotes o^{th} agent's location arbitrarily chosen from the agents, and $V1 \neq o$.

The Piranha Population Survival Strategies

To handle, the survival rate Sv_R of the piranha is determined via Equation (24). If, the survival rate is $Sv_R \leq 1/4$, then the population is renewed via Equation (25).

$$Sv_R(o) = \frac{Max_{fit} - fit(o)}{Max_{fit} - Min_{fit}} \quad (24)$$

$$c_o(y+1) = c_{py}(y) + \frac{1}{2}\left\{\begin{array}{l}\left[c_{V1}(y) - R * c_{V2}(y)\right] - \\ \left[c_{V2}(y) - R * c_{V3}(y)\right]\end{array}\right\} \quad (25)$$

Here, the terms $c_{v1}(y)$, $c_{v2}(y)$, $c_{v3}(y)$ denote the positions of the agent V1, V2, V3 arbitrarily determined from the piranhas $V1 \neq V2 \neq V3$ correspondingly.

The pseudocode of PFOA is given in Algorithm. 3.

Algorithm 3: Traditional PFOA

Initialize the parameters

$K = 0.5$, it denotes the possibility that piranha is hungry and the possibility that they are in the scavenging foraging pattern or attack pattern.

$B = 0.75$, it the possibility of blood concentration in the piranha to evaluate which attack pattern is performed (bloodthirsty cluster attack pattern or the localized group attack)

Setup the initial population

While $iteration < M_x itr$ do

  If $random < K$ then

    Upgrade the non-linear cosine factor D via Equation (19)

      If $random < B$ then

        Evaluate the parameter of blood concentration G_o through Equation (17)

        Pattern 1: localized group attack pattern via Equation (21)

      Else

        Pattern 2: bloodthirsty cluster attack pattern via Equation (22)

      End if

Else

    Pattern 3: scavenging foraging pattern via Equation (24)

    End if

    Upgrade the survival rate of the piranha, when is less through Equation (25)

    Evaluate C_{Nw}, the latest search agent's fitness function

    If $C_{Nw} < C_{py}$ then

      Set $C_{py} = C_{Nw}$

    End if

    Set $iteration = iteration + 1$

End while

Stop criteria fulfilled

Display C_{Py} and the best value

End

5. Efficient Channel Estimation Using Adaptive and Attention-Based Deep Learning Mechanism in MIMO-NOMA for mmWave Systems

5.1. Channel Attribute Generation

The introduced Ada-ACAE-based channel estimation framework is performed with the channel matrix as the input for estimating the channel that is obtained under the environment, as discussed in Table 1.

Table 1. Dataset creation parameters

Parameters	Values
Number of Sub Carriers	K = [2, 4, 6, 8, 10, 12]
Number of Antennas	[5, 10, 15, 20, 25]
Total Bandwidth	5
System Delay Requirement	1
Circuit Power	30
Antenna Power	27
Power Amplifier Coefficient	0.38
Maximum No. of Users	50
Initial Energy	0.5
Distances	d1 = 500, d2 = 200
Power Allocation Coefficients	a1 = 0.75, a2 = 0.25
Path Loss Exponent	4
Target Rates	R1 = 1, R2 = 3
Transmit Power (in dbm)	Pt = [-30, -25, -20, -15, -10, -5, 0, 10, 20, 30]

5.2. Convolutional Autoencoder

An Auto Encoder (AE) is employed to attain the feature vector by employing an "encoder-decoder module". The encoder compresses the input signal into significant features, and the decoder rebuilds the compressed information and offers an output that resembles the input signal. Auto-encoder is compressed of "input layer, hidden layer, and output layer".

At the beginning, the input signal is offered into the encoder phase with less dimension and later given to the decoder. Dimension of the input signal is minimized via training the output layer and later, offered to the hidden layer. The input signal is denoted by the term Q, and the encoded outcome attained from the encoder phase is expressed by Equation (26).

$$E_d = t(x) = \beta(WX + b_x) \tag{26}$$

In Equation (29), the activation function is denoted by the term β. The input signal is then reassembled at the decoder phase via Equation (27).

$$X_1 = g(q) = \alpha(W + b_y) \tag{27}$$

In Equation (27), the sigmoid activation function of the decoder is indicated by the term α, and the decoder variable's biasing vectors are represented by the terms b_x and b_y. During the reconstruction, there is a risk of data loss. To resolve this issue, the autoencoder is rained by the variables ϕ = (W, b_y, b_x). It is numerically shown in Equation (28).

$$\eta = \min_{\phi} L(X, X') = \min_{\phi} L(X, g(f(x))) \tag{28}$$

The frequent and random loss of information is evaluated by the cross-entropy function and also via square error value, correspondingly as shown in Equation (29).

$$L(\phi) = \sum_{i=1}^{n} [x_u \log(y_u) + (1 - x_u)\log(1 - y_u)] \tag{29}$$

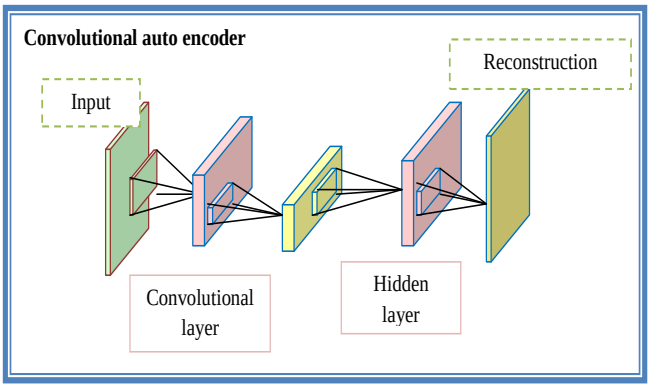

Fig. 5 Architectural representation of convolutional auto encoder

Employing auto-encoders in channel estimation offers certain merits by minimizing the challenges of the traditional channel estimation approaches and enhancing the accuracy during estimation. Information loss is a major demerit of the autoencoder. It can be resolved by embedding a convolution layer in the encoder phase of the auto-encoder. This layer is capable of attaining specific features from the signal that can be employed for channel estimation. The outcome attained from the convolutional layer is a feature map that can flatten and be associated with the decoder part of the auto encoder. The architectural illustration of the convolutional auto-encoder is presented in Figure 5.

5.3. Ada-ACAE-Based Channel Estimation

In this introduced model, channel estimation is performed on the developed Ada-ACAE framework. The tuned pilot design is given to the Ada-ACAE model. The tuned pilot signals are employed to attain the parameters of the channel and also to train the framework by employing a deep learning technique.

The Ada-ACAE model is developed by embedding an attention mechanism on the CAE. It improves the channel estimation by concentrating on the necessary features of the signal at the time of encoding and decoding procedure.

By integrating the attention mechanisms, the convolutional auto-encoder is capable of attaining the difficult relations within the input data for effective estimation. The attention mechanism assists the auto-encoder in assigning its resources accurately and achieving the most relevant information necessary to implement channel estimation in MIMO-NOMA networks. In this implemented channel estimation framework, the CSI matrix is taken as the input for channel estimation.

Next, the frequency feature vectors presented in the CSI matrix are extracted using the AE filters. The Ada-ACAE model determines a channel response as an output for channel estimation. The introduced WH-PFOA is employed to upgrade the pilot symbols employed on the Ada-ACAE network to increase effective channel estimation. A diagrammatic illustration of the developed Ada-ACAE-aided Channel Estimation framework is shown in Figure 6.

5.4. Objective of Channel Estimation Model

In the proposed Ada-ACAE-aided channel estimation model, the optimal pilot designs tuned by the implemented WH-PFOA are employed to enhance the efficiency of channel estimation. The Ada-ACAE parameters, such as activation function, number of hidden neurons, and epoch, are tuned via the implemented WH-PFOA for minimizing the "Bit Error Rate (BER) and Mean Squared Error (MSE)". The major objectives of the Ada-ACAE-based channel estimation model are described in Equation (30).

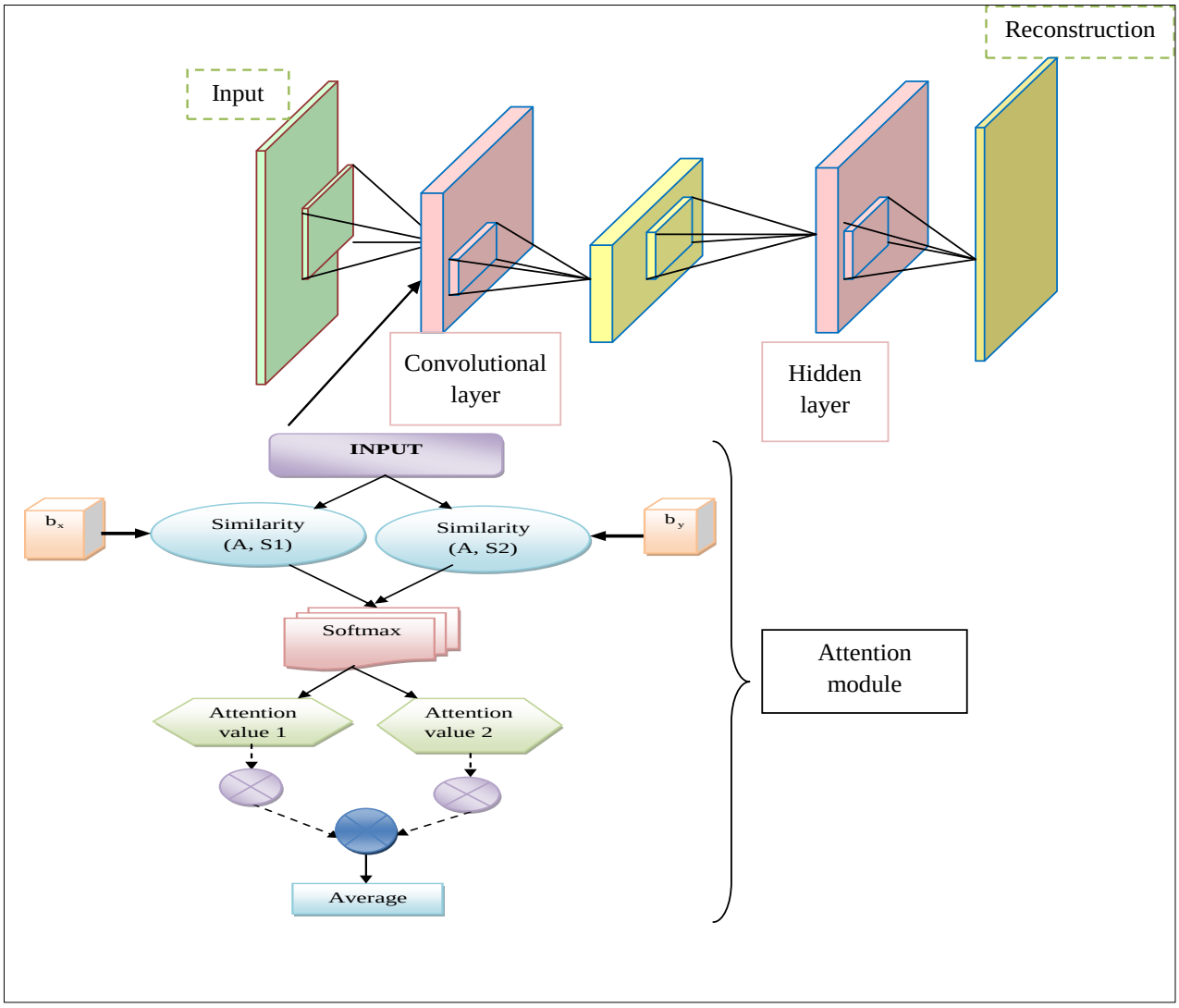

Fig. 6 Diagrammatic illustration of Ada-ACAE-based channel estimation framework

$$Obj = \underset{\left\{Ac_L^{Ada\text{-}ACAE}, Ec_N^{Ada\text{-}ACAE}, Hn_V^{Ada\text{-}ACAE}\right\}}{\arg\min} \left(BER + MSE\right) \quad (30)$$

Here, the hidden neuron's count in the Ada-ACAE is represented by the term $Hn_V^{Ada\text{-}ACAE}$ that lies between in the interval [5,255], the activation function of the Ada-ACAE is indicated by the term $Ac_L^{Ada\text{-}ACAE}$ that lies between [1,5], and the number of epochs in Ada-ACAE is denoted by the term $Ec_N^{Ada\text{-}ACAE}$ that ranges between [5,50]. BER is the "calculation of the bit count that is attained in error compared to the overall bits transmitted on the communication model". It is evaluated using Equation (31).

$$BER = \frac{T_{Bit}}{O_{bit}} \quad (31)$$

Here, the entire bit converted in the framework is indicated as Obit, and the total count of bits attained with error is expressed as T_{Bit}. MSE defines the "average square difference between the estimated and the actual value." The MSE is arithmetically presented via Equation (32).

$$MSE = \frac{1}{b}\sum_{u=1}^{b}\left(T_u - \hat{T}_u\right)^2 \quad (32)$$

Here, the data point's count is denoted by the term b and the value observed and predicted is expressed by the terms T_u and $\hat{T}_u$.

6. Result and Discussion

6.1. Experimental Setup

The proposed Ada-ACAE framework was executed in MATLAB2020a. Particularly, the carrier frequency employed in the mmWave system is chosen as 28GHz, and the bandwidth's standard value is taken as 1GHz for experimentation. This network considered the highest

iteration count as 50, population counts as 10, and length of chromosome as 3 for channel estimation.

The efficiency of the developed channel estimation scheme is investigated with few optimization approaches like "Clouded Leopard Optimization (CLO) - Ada-ACAE [29], Walrus Optimization Algorithm (WOA) - Ada-ACAE [30], Wild Horse Optimization Algorithm (WHOA) - Ada-ACAE [26] and Piranha Foraging Optimization Algorithm (PFOA)-Ada-ACAE [27] and estimation approaches like FCFGS-CV [19], Mixed ADC [20], LDAMP [23]. The simulation parameters employed in this developed model are depicted in Table 2.

Table 2. Simulation parameters

Parameters	Values
Symbol's time period	171ms
Channel Bandwidth	1 GHz
CP Length	10 ms
RF chains count	4
Pilot count	200
Carrier frequency	28 GHz
The number of BS antenna	64
Small cell coverage	500

6.2. Performance Measure

The performance metrics employed in this channel estimation model are discussed below. Performance indices like Mean Error Percentage (MEP), Symmetric Mean Absolute Percentage Error (SMAPE), Mean Absolute Scaled Error (MASE), Mean Absolute Error (MAE), and Root Mean Square Error (RMSE) were used to find the efficacy of the developed model.

(a) MEP is derived via Equation (33).

$$\mathrm{MEP}=\frac{100\%}{\mathrm{B}}\sum_{\mathrm{V}=1}^{\mathrm{B}}\frac{\mathrm{sv}-\mathrm{gv}}{\mathrm{sv}} \tag{33}$$

(b) SMAPE can be expressed through Equation (34).

$$\mathrm{SMAPE}=\frac{100\%}{\mathrm{dq}}\sum_{\mathrm{R}=1}^{\mathrm{dq}}\frac{|\mathrm{gv}-\mathrm{sv}|}{\frac{(|\mathrm{sv}|+|\mathrm{gv}|)}{2}} \tag{34}$$

(c) MASE is expressed by Equation (35).

$$\mathrm{MASE}=\mathrm{mean}\left(\frac{|\mathrm{gv}|}{\frac{1}{\mathrm{dq}-1}\sum_{\mathrm{R}=1}^{\mathrm{dq}}|\mathrm{sv}_{\mathrm{R}}-\mathrm{sv}_{\mathrm{R}-1}|}\right) \tag{35}$$

(d) MAE is defined through Equation (36).

$$\mathrm{MAE}=\frac{\sum_{\mathrm{R}=1}^{\mathrm{dq}}|\mathrm{gv}_{\mathrm{R}}-\mathrm{sv}_{\mathrm{R}}|}{\mathrm{dq}} \tag{36}$$

(e) RMSE can be derived through Equation (37).

$$\mathrm{RMSE}=\sqrt{\frac{\sum_{\mathrm{R}=1}^{\mathrm{dq}}(\mathrm{gv}_{\mathrm{R}2}-\mathrm{gv}_{\mathrm{R}1})^2}{\mathrm{dq}}} \tag{37}$$

(f) L1-Norm is arithmetically derived via Equation (38).

$$\mathrm{Z}_{\mathbf{1}}=\sum_{\mathrm{R}}|\mathrm{Z}_{\mathrm{R}}| \tag{38}$$

(g) L2-Norm is derived by Equation (39).

$$\mathrm{Z}\mathbf{2}=\left(\sum_{\mathrm{R}=1}^{\mathrm{dq}}\mathrm{Z}_{\mathrm{R}}^2\right)^{\frac{1}{2}} \tag{39}$$

(h) L-Infinity Norm can be numerically expressed by Equation (40).

$$\mathrm{J}_{\mathbf{inf}}=\max_{1\le \mathrm{R}\le \mathrm{dq}}|\mathrm{J}_{\mathrm{R}}| \tag{40}$$

Here, the actual value is indicated by the term SV, and the forecasted value is denoted via gv the calculation element that is integrated for all suited points is denoted by the term R, the matrix form is represented by the term N, and the matrix size is represented by the term dq, where, R=1,2,…dq.

6.3. Efficiency Examination for Introduced Ada-ACAE-Based Channel Estimation Network in Terms of Heuristic Approaches

Figure 7 demonstrates the accuracy of the channel estimation network while comparing the generated model with various heuristic techniques. Figure 7(a) shows that the generated framework better CLO-Ada-ACAE, WOA-Ada-ACAE, WHOA - Ada-ACAE, and PFOA Ada-ACAE by .57%, 30%, 53.33%, and 39.13%, respectively, by considering the value of step per epoch as 200. The RMSE and MASE values of the proposed framework are decreased at the 200th step per epoch. This proved that the channel estimation performance of the developed framework attained better results than the conventional techniques. The lower values of error metrics showed that the suggested model detect the effective channel that received information with no information loss and high BER. The detected channel, by using the developed model, helps the user to perform the lossless communication process. Thus, the introduced channel estimation model shows enhanced effectiveness in determining the exact channel with improved reliability.

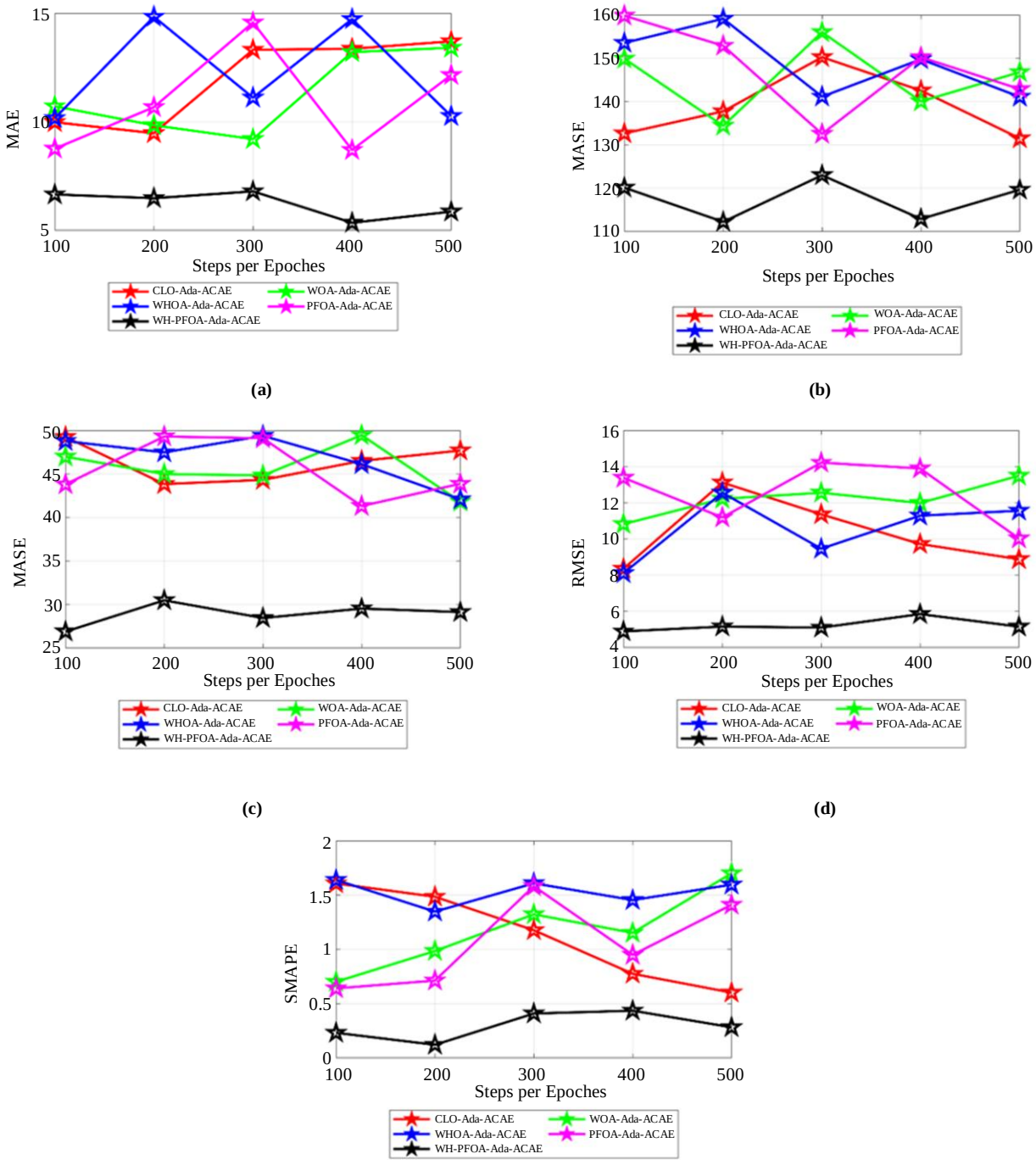

(a) **(b)** **(c)** **(d)** **(e)**

Fig. 7 Efficiency evaluation of introduced finger vein-based authentication framework on the basis of Heuristic approaches in terms of (a) MAE, (b) MASE, (c) MEP, (d) RMSE, and (e) SMAPE.

6.4. Effectiveness Examination of the Developed Model Based on Channel Estimation Techniques

Figure 8 represents the performance of the implemented model with various channel estimation mechanisms. Figure 7(b) conveys that the proposed network exceeds the authentication models such as FCFGS-CV, Mixed ADC, LDAMP, and Ada-ACAE by 27.86%, 21.42%, 20.28%, and 27.15% correspondingly, by considering the value of step per epoch as 200. When considering all error metrics like MAE, MASE, MEP, RMSE, and SMAPE, the proposed model attained very low values at all steps per epoch values. The lower error values eliminate the imperfect channel estimation,

and it satisfies the user requirement in the communication process. Here, the impact of the Ada-ACAE in the channel estimation is determined using various error metrics. When increasing the steps per epoch, the error values of the developed model show slight variation. However, the error values are comparatively lower than the existing techniques. These results showed that the developed Ada-ACAE provides excellent effects in the channel estimation process. Hence, the introduced channel estimation network offers more advanced performance than the traditional approaches.

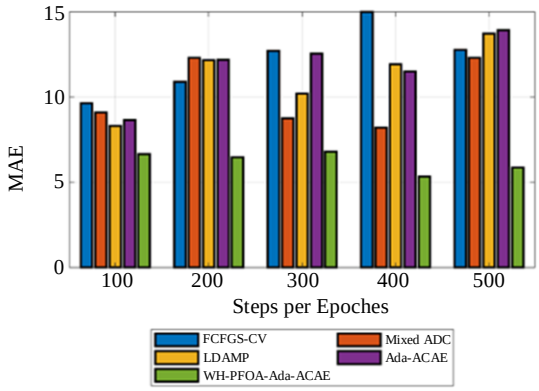

(a)

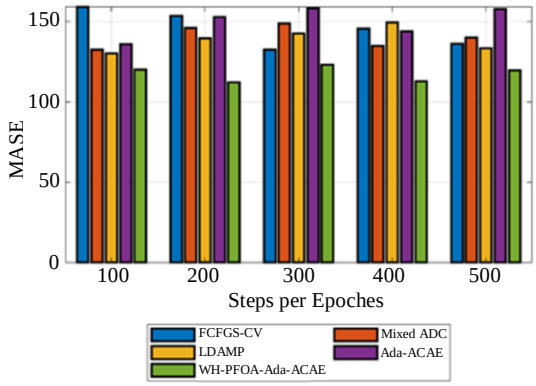

(b)

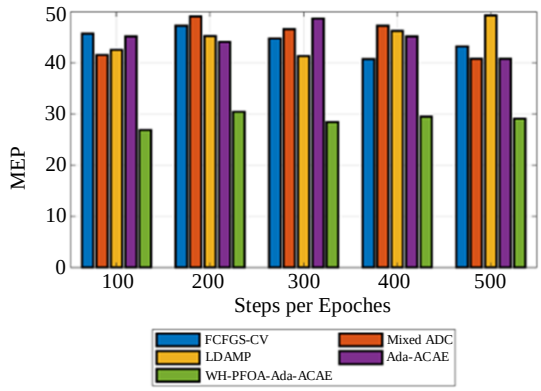

(c)

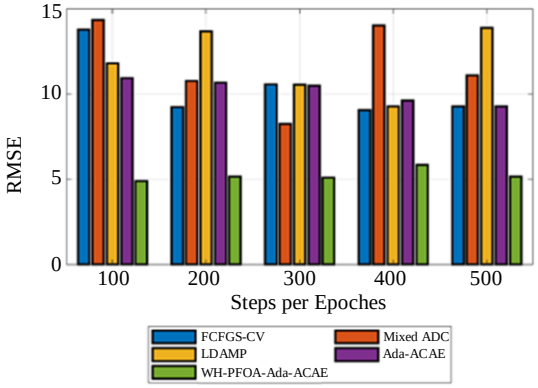

(d)

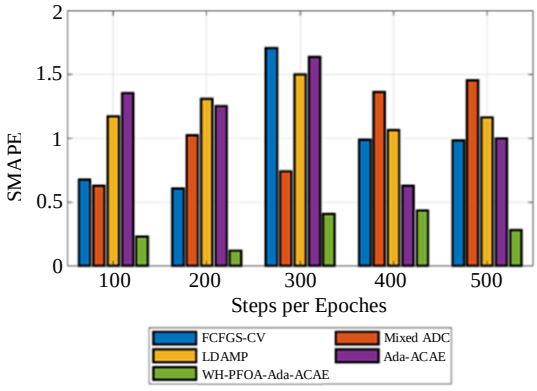

(e)

Fig. 8 Effectiveness examination of the developed model based on authentication techniques for Dataset 1 and Dataset 2 in terms of (a) MAE, (b) MASE, (c) MEP, (d) RMSE, and (e) SMAPE.

6.5. Convergence Performance of the Introduced Scheme

Figure 9 demonstrates the convergence evaluation of the generated channel estimation model. On the basis of Figure 9(a), the introduced model shows enhanced performance than CLO, WOA, WHOA, and PFOA by 4.34%, 8.33%, 5.17%, and 6.77%, respectively, by considering the iteration count 10. 9. The convergence results showed that the cost function of the developed model is lower than existing algorithms and it achieved the global optimal solution at an earlier stage. The convergence results showed that the suggested model does not stick in the local optimal condition, and it converges faster than the traditional algorithm to provide an optimal solution. Therefore, the generated network attains enhanced performance than other traditional systems.

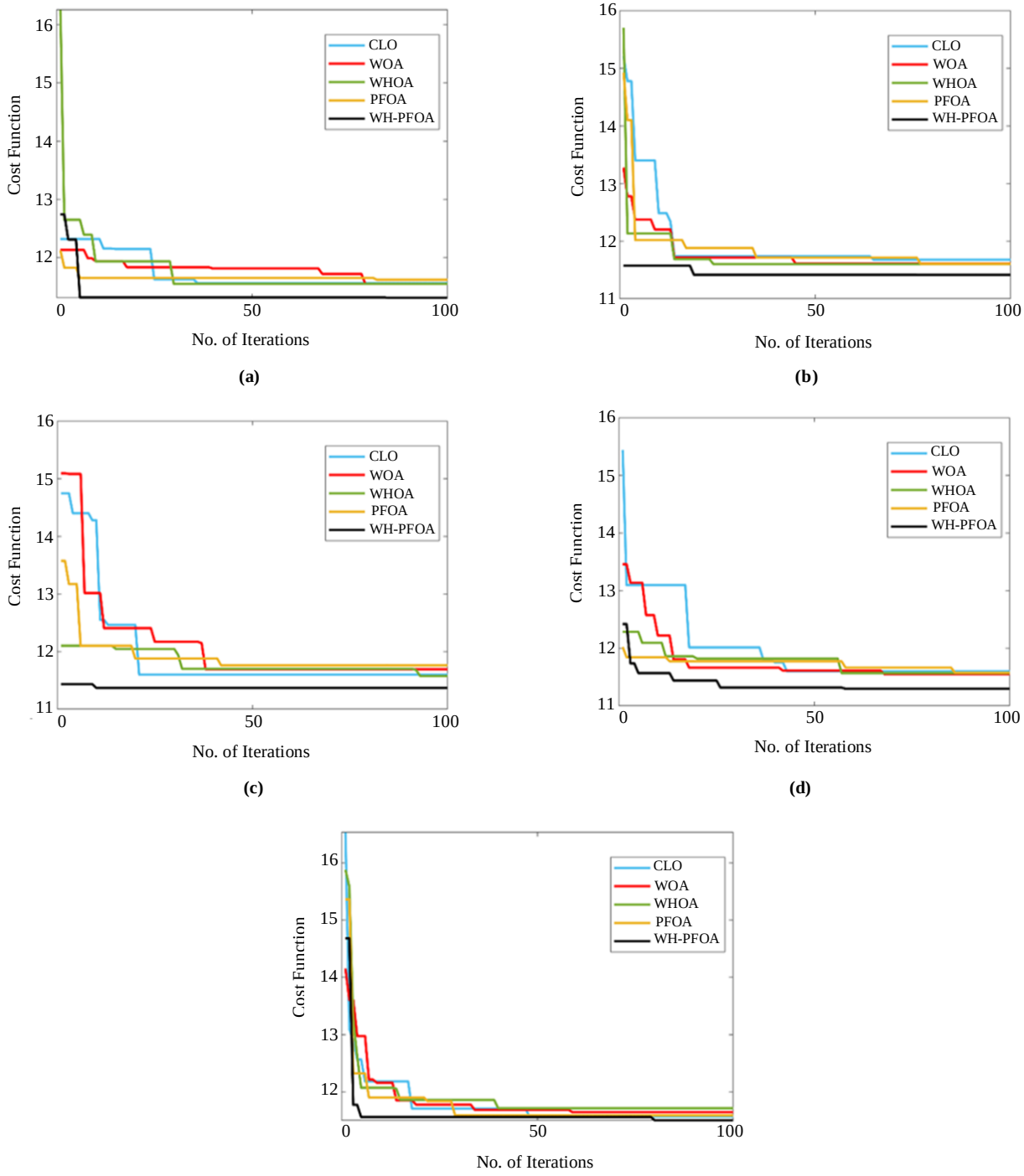

Fig. 9 Convergence performance of the introduced model

6.6. Performance Evaluation of Channel Estimation by Considering the Maximum Power

Figure 10 demonstrates the performance evaluation of channel estimation by considering the max power. Based on Figure 10(a), the introduced model shows enhanced performance than Gradient descent, FCFGS-CV, Mixed ADC, and LDAMP by 56.92%, 46.15%, 23.07%, and 12.30%, respectively, by considering the maximum power as 10.9. The proposed scheme's spectral efficiency, BLER, throughput, and effective achievable rate are higher than the conventional techniques. The improved values of spectral efficiency, BLER, and throughput showed that the suggested model determines the ideal channel for performing the lossless communication process.

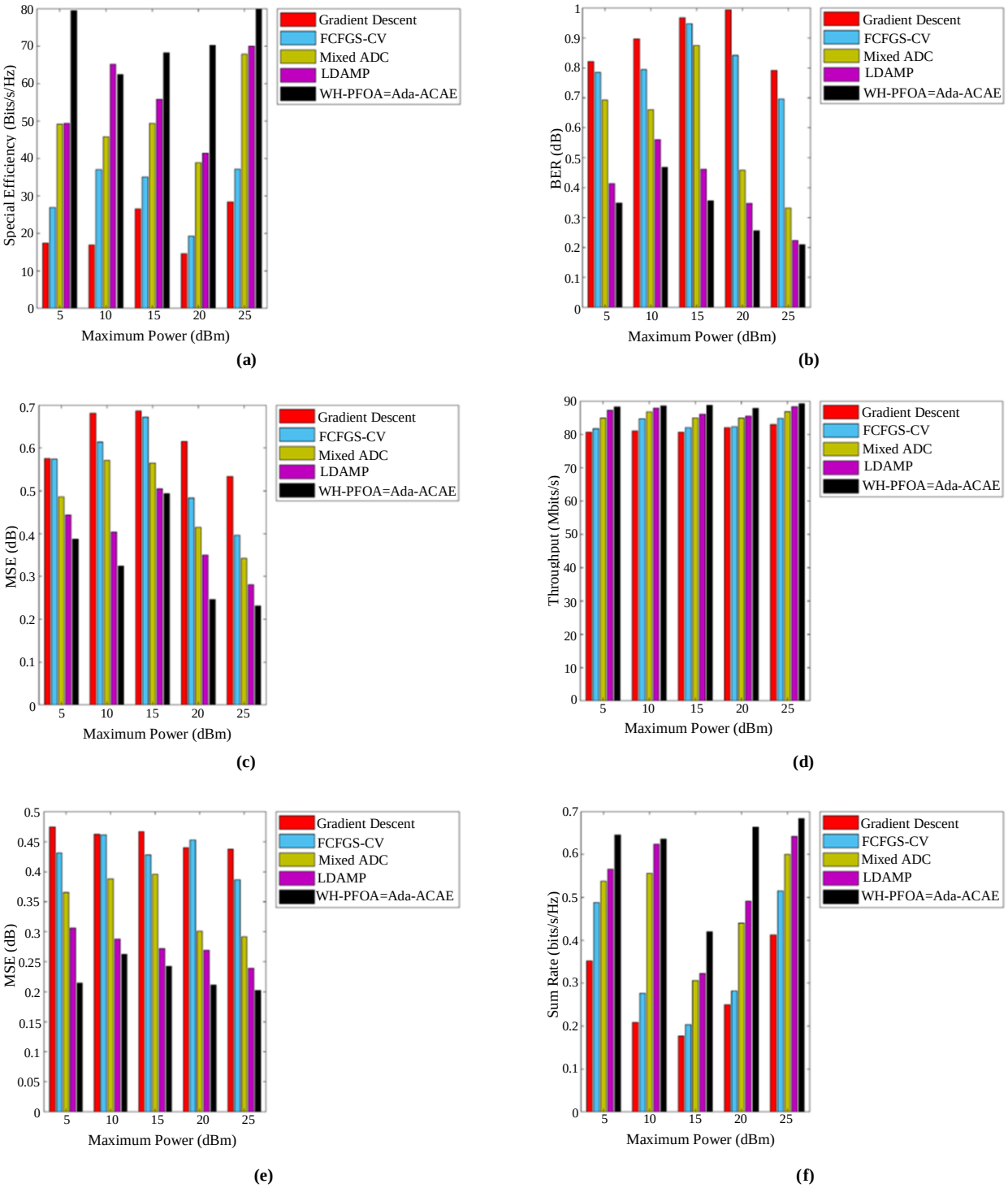

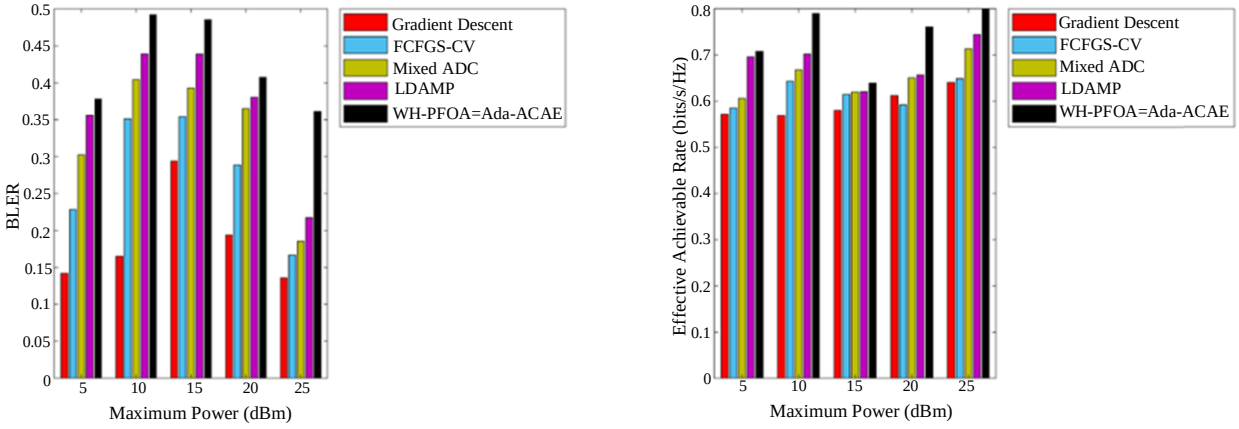

(g) **(h)**

Fig. 10 Performance evaluation of channel estimation by considering the max power in terms of (a) Spectral efficiency, (b) BER, (c) MSE, (d) Throughput, (e) NMSE, (f) Sum Rate (g) BLER, and (h) Effective achievable rate.

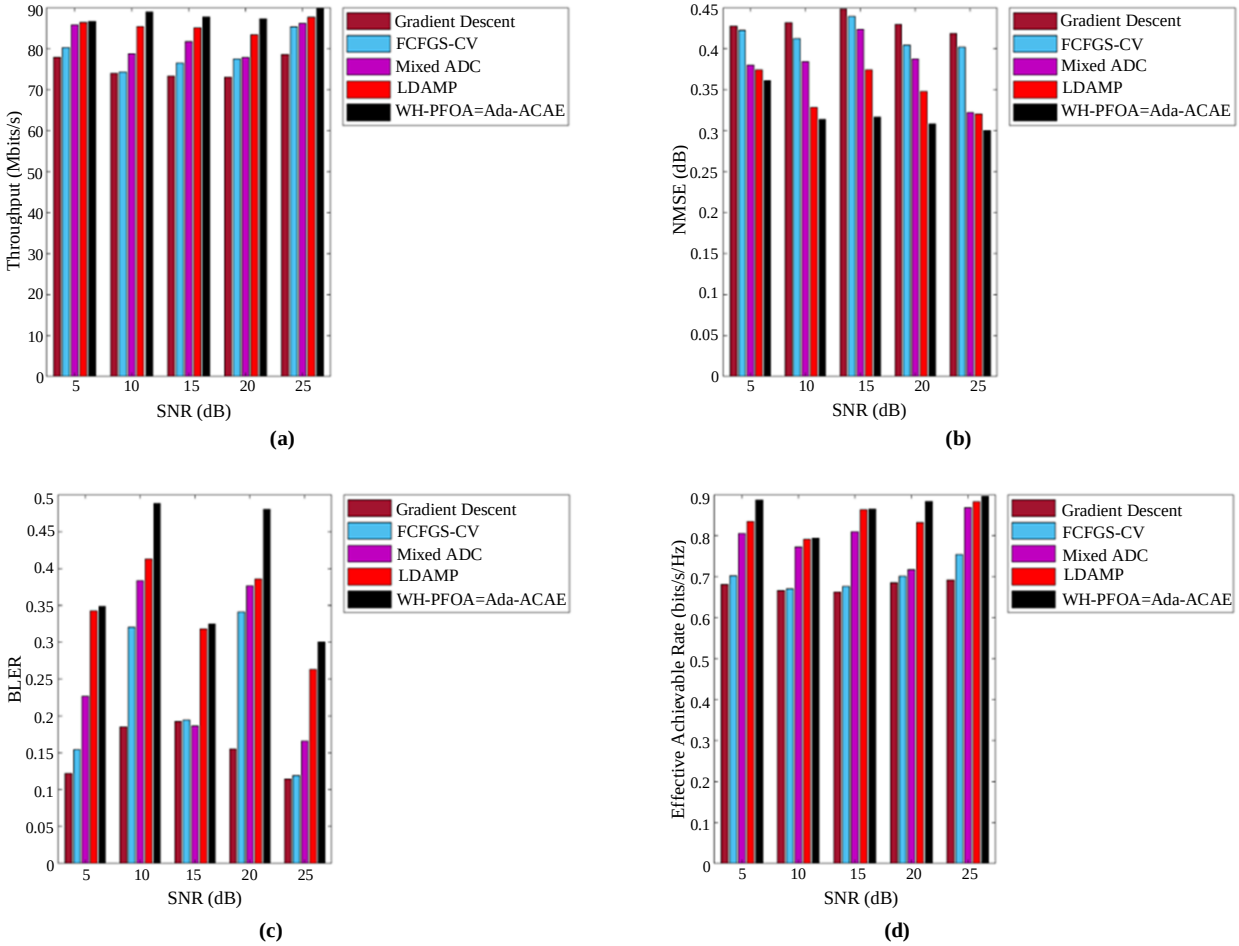

(a) **(b)**

(c) **(d)**

Fig. 11 Performance evaluation of channel estimation by varying SNR in terms of (a) Throughput, (b) NMSE, (c) BLER, and (d) Effective achievable rate.

Likewise, the MSE, BER, and NMSE of the suggested model are lower than the existing techniques. These results proved that the suggested model provides a robust and efficient channel for the effective communication process. The improvement in the throughput and maximum achievable rate eliminates the hitches involved in the communication process. Moreover, the enhanced value of efficiency, BLER, and throughput values fulfill the requirements of the

communication system. Therefore, the implemented model attains enhanced performance in channel estimation than other existing approaches.

6.7. Performance Evaluation of Channel Estimation by Varying SNR

Figure 11 demonstrates the performance assessment of channel estimation by varying SNR. Based on Figure 11(a), the introduced model shows enhanced performance than Gradient descent, FCFGS-CV, Mixed ADC, and LDAMP by 1.36%, 2.77%, 5.71%, and 4.81%, respectively, by considering the SNR value -20. For different values of SNR, the NMSE and BLER of the proposed model is lower while the throughput and effective achievable rate of the proposed scheme is higher than the other techniques. These results confirmed that the developed model accurately detects the channel for enhancing the energy and the spectral efficiency values. Therefore, the implemented model attains enhanced performance in channel estimation than other existing frameworks.

6.8. Performance Evaluation of Channel Estimation by Considering User Count

Figure 12 demonstrates the performance evaluation of channel estimation by considering the user count. Based on Figure 12(a), the introduced model shows enhanced performance than Gradient descent, FCFGS-CV, Mixed ADC, and LDAMP by 81.81%, 62.16%, 36.36%, and 1.69%respectively, by considering the user count as 5. The spectral efficiency, throughput, and BLER are the positive metrics, and the enhancement in these positive metrics proved that the suggested model detects the channel for performing the efficient communication process with high spectral efficiency. The results showed that the developed model flexibly determines the channel with high accuracy, which enhances the communication performance. The obtained results showed that the suggested model accurately detects the channel and improves the capability of the wireless communication system. Therefore, the implemented model attains enhanced performance in channel estimation than traditional systems.

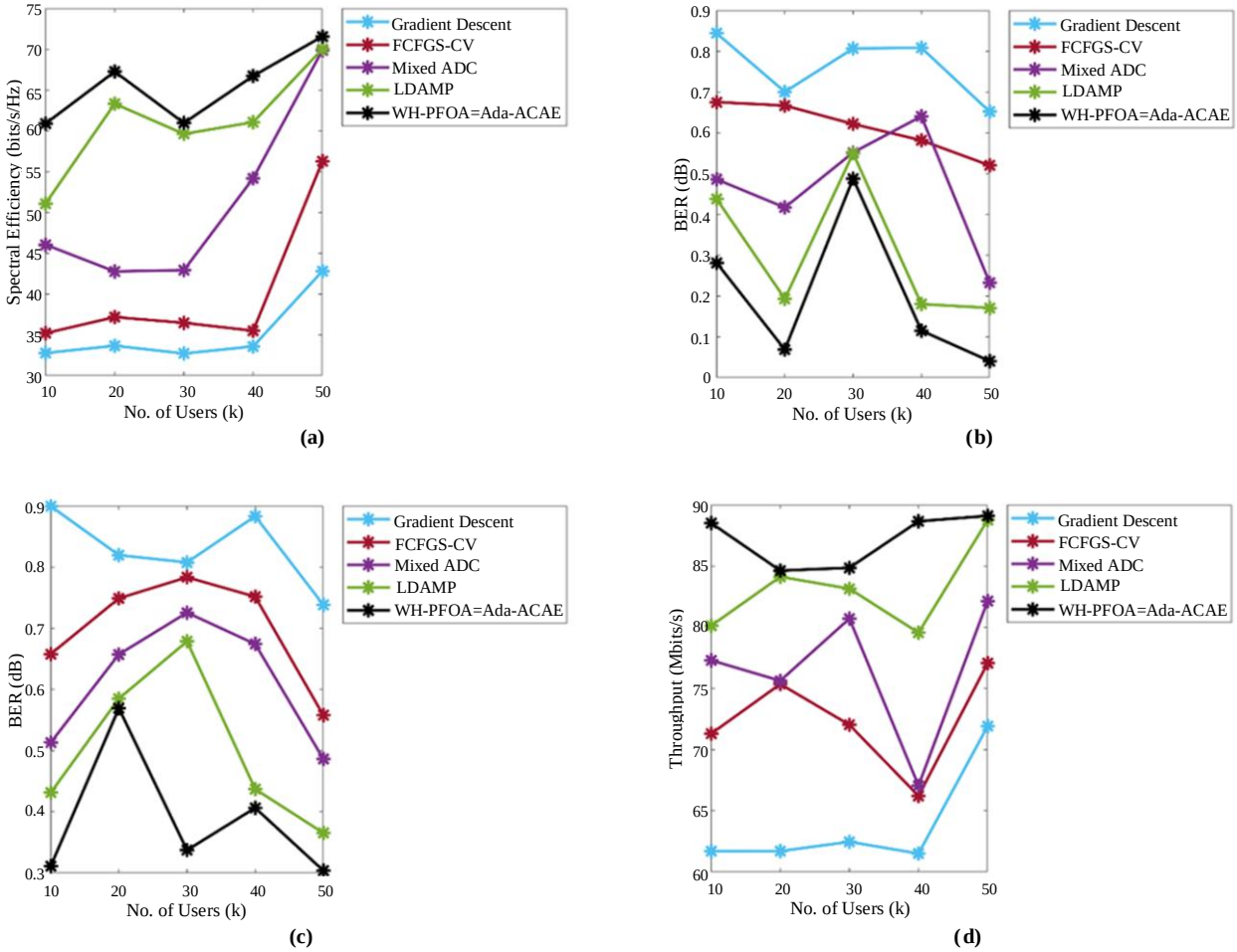

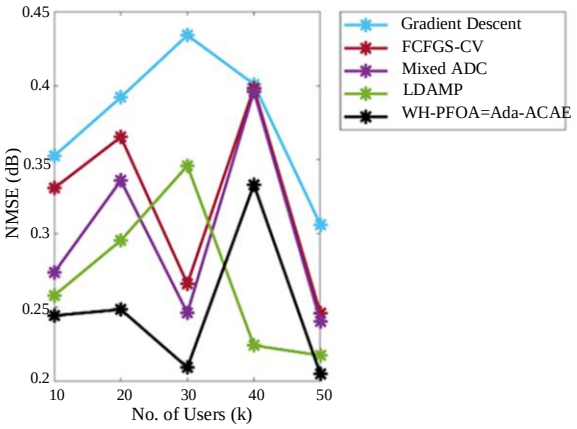

(e)

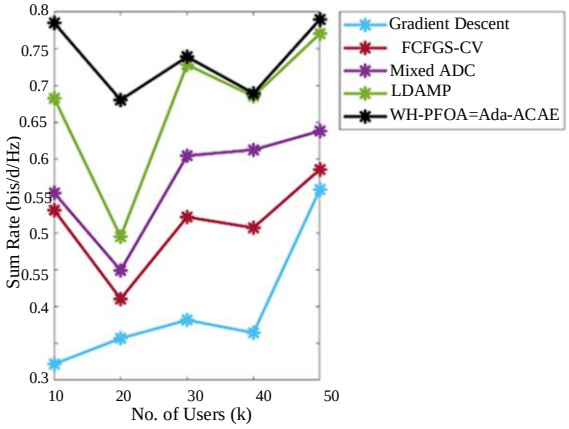

(f)

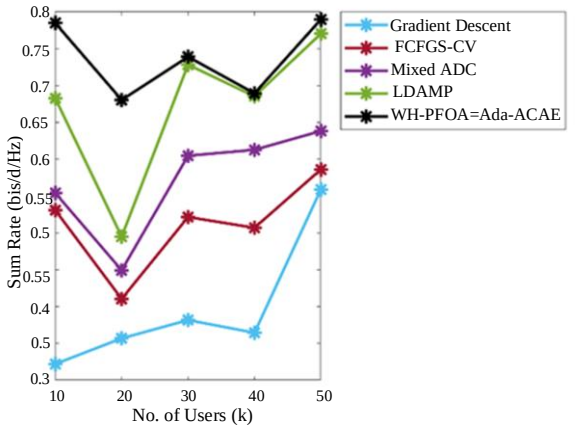

(g)

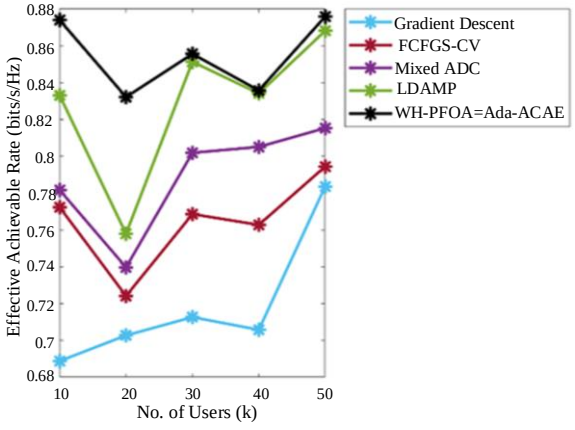

(h)

Fig. 12 Performance evaluation of channel estimation by considering the User count in terms of (a) Spectral efficiency, (b) BER, (c) MSE, (d) Throughput, (e) NMSE, (f) Sum Rate (g) BLER, and (h) Effective achievable rate.

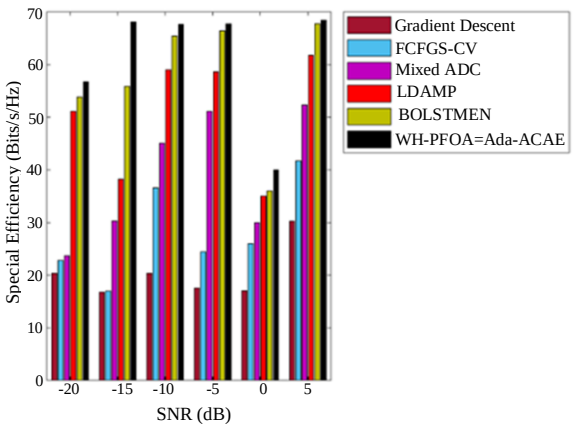

(a)

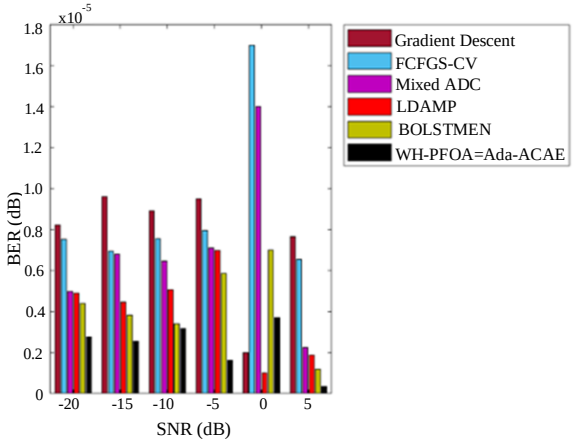

(b)

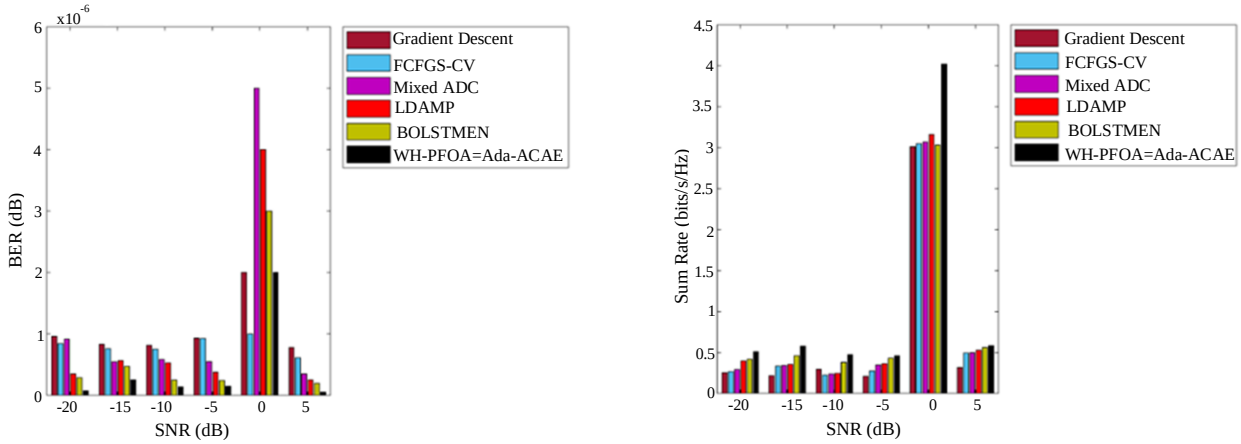

(c) **(d)**

Fig. 13 Performance evaluation of channel estimation by varying SNR in terms of (a) Spectral efficiency, (b) BER, (c) MSE, and (d) Sum rate.

6.9. SNR-Based Comparative Analysis with Channel Estimation Techniques

Figure 13 conveys the comparative analysis of the developed model by varying SNR. Based on Figure 13(a), the introduced model shows enhanced performance than Gradient descent, FCFGS-CV, Mixed ADC, LDAMP and BOLSTMEN by 65.51%, 60.344%, 58.62%, 10.34%, and 6.89%, respectively, by considering the SNR value -20. The proposed model achieved higher spectral efficiency and sum rate values but it achieved lower MSE and BER values. These results proved that the channel estimation performance of the developed model is more sensitive than the other techniques. The estimated channel using the developed approach fulfils the growing need for wireless data traffic. The maximization of spectral efficiency enhances the reliability of the MIMO-NOMA. Therefore, the implemented model attains enhanced performance in channel estimation than other existing frameworks.

6.10. Overall Efficiency Examination of the Generated Framework Based on Heuristic Approaches

Table 3 presents the effectiveness of the generated channel estimation scheme with various heuristic approaches. On the basis of Table 3, the MEP of the introduced channel estimation network conveys enhanced performance than CLO-Ada-ACAE, WOA-Ada-ACAE, WHOA - Ada-ACAE, and PFOA Ada-ACAE by 38.94%, 30.36%, 30.80%, and 33.62%, respectively. Thus, the generated channel estimation achieves superior performance than existing approaches.

Table 3. Overall efficiency examination of the generated framework based on Heuristic approaches

TERMS	CLO [29]	WOA [30]	WHOA [26]	PFOA [27]	WH-PFOA
MEP	47.71	41.83	42.10	43.89	29.13
SMAPE	0.60	1.70	1.60	1.41	0.28
MASE	131.49	146.81	141.09	142.89	119.63
MAE	13.71	13.42	10.27	12.16	5.86
RMSE	8.88	13.50	11.56	10.03	5.15
L1-NORM	577.61	605.98	557.86	650.99	442.77
L2-NORM	81.64	80.20	80.83	82.76	74.45
L-INF-NORM	14.69	15.27	15.06	17.80	11.60

6.11. Overall Performance Evaluation of the Proposed Scheme Based on Several Channel Estimation Techniques

Table 4 presents the performance examination of the generated channel estimation model with various estimation approaches. The table shows that the introduced system exhibits improved accuracy than other authentication approaches like CFGS-CV, Mixed ADC, LDAMP, and Ada-ACAE by 71.42%, 80.68%, 75.86%, and 72%, respectively. Therefore, the generated estimation model is more effective than the existing channel estimation models.

6.12. Statistical Evaluation of the Developed Model

Table 5 demonstrates the statistical evaluation of the introduced model. Based on the table, the best performance of the developed authenticated approach exceeds CLO, WOA, WHOA, and PFOA by 2.24%, 2.07%, 2.07%, and 2.66%, respectively. On the basis of the attained outcome, the developed estimation attains improved performance than other traditional models.

Table 4. Overall performance evaluation of the proposed model with existing Channel Estimation Techniques

TERMS	FCFGS-CV [19]	Mixed ADC [20]	LDAMP [23]	Ada-ACAE [28]	WH-PFOA Ada-ACAE
MEP	43.26	40.81	49.30	40.82	29.13
SMAPE	0.98	1.45	1.16	1.00	0.28
MASE	136.19	140.05	133.32	157.74	119.63
MAE	12.77	12.31	13.72	13.92	5.86
RMSE	9.28	11.09	13.88	9.27	5.15
L1-NORM	569.91	654.89	633.82	665.87	442.77
L2-NORM	85.09	85.01	82.72	82.20	74.45
L-INF-NORM	14.40	15.17	16.14	16.50	11.60

Table 5. Statistical evaluation of the proposed Channel Estimation Network

Algorithms	CLO [29]	WOA [30]	WHOA [26]	PFOA [27]	WH-PFOA
Number of Nodes: 10					
Best	11.57	11.55	11.55	11.62	11.31
Worst	12.32	12.14	16.25	12.13	12.74
Mean	11.73	11.79	11.76	11.66	11.38
Median	11.57	11.82	11.55	11.65	11.32
Standard Deviation	0.28	0.16	0.54	0.06	0.26
Number of Nodes: 20					
Best	11.68	11.61	11.60	11.61	11.42
Worst	15.21	13.28	15.70	14.92	11.57
Mean	11.94	11.75	11.71	11.84	11.44
Median	11.74	11.61	11.60	11.72	11.42
Standard Deviation	0.68	0.29	0.44	0.47	0.06
Number of Nodes: 30					
Best	11.60	11.69	11.58	11.76	11.37
Worst	14.75	15.09	12.10	13.57	11.43
Mean	11.98	12.12	11.80	11.91	11.37
Median	11.60	11.69	11.70	11.76	11.37
Standard Deviation	0.88	0.84	0.18	0.35	0.02
Number of Nodes: 40					
Best	11.60	11.55	11.57	11.57	11.30
Worst	15.44	13.46	12.28	12.02	12.42
Mean	11.97	11.76	11.75	11.72	11.38
Median	11.60	11.61	11.82	11.77	11.32
Standard Deviation	0.64	0.43	0.20	0.09	0.18
Number of Nodes: 50					
Best	11.57	11.65	11.72	11.60	11.51
Worst	16.53	14.15	15.88	15.36	14.68
Mean	11.79	11.83	11.90	11.76	11.62
Median	11.57	11.69	11.72	11.60	11.57
Standard Deviation	0.56	0.43	0.59	0.55	0.44

7. Conclusion

An effective channel estimation model for the mmWave networks to attain increased information rate, reliability, and efficiency through the usage of deep learning techniques. Initially, beam forming is performed based on the introduced WH-PFOA to minimize the network complexity and also to perform effective channel estimation on the MIMO network.

The attained beam was fed into the introduced Ada-ACAE network for channel estimation. The introduced WH-PFOA strategy optimized the parameters obtained on the Ada-ACAE model. The attained outcome was estimated via classic meta-heuristic strategies and various channel estimation models to showcase their effectiveness. The BER of the developed model is higher than Gradient descent, FCFGS-CV, Mixed ADC, and LDAMP by 84.28%, 84.05%, 75.55%, and 45% respectively.

The MAE of the developed model for channel estimation exceeds the performance of the traditional models such as CLO-Ada-ACAE, WOA-Ada-ACAE, WHOA-Ada-ACAE, and PFOA-Ada-ACAE by 57.25%, 56.33%, 42.94%, and 51.80%, correspondingly. Thus, the suggested Ada-ACAE network achieved superior performance in effective channel estimation and also improved the reliability and performance of the mmWave network.

References

[1] Bingtong Xiang, Die Hu, and Jun Wu, "Deep Learning-Based Downlink Channel Estimation for FDD Massive MIMO Systems," *IEEE Wireless Communications Letters*, vol. 12, no. 4, pp. 699-702, 2023. [CrossRef] [Google Scholar] [Publisher Link]

[2] Chang-Jae Chun, Jae-Mo Kang, and Il-Min Kim, "Deep Learning-Based Channel Estimation for Massive MIMO Systems," *IEEE Wireless Communications Letters*, vol. 8, no. 4, pp. 1228-1231, 2019. [CrossRef] [Google Scholar] [Publisher Link]

[3] Byungju Lim et al., "Joint Pilot Design and Channel Estimation Using Deep Residual Learning for Multi-Cell Massive MIMO Under Hardware Impairments," *IEEE Transactions on Vehicular Technology*, vol. 71, no. 7, pp. 7599-7612, 2022. [CrossRef] [Google Scholar] [Publisher Link]

[4] Mehran Soltani, Vahid Pourahmadi, and Hamid Sheikhzadeh, "Pilot Pattern Design for Deep Learning-Based Channel Estimation in OFDM Systems," *IEEE Wireless Communications Letters*, vol. 9, no. 12, pp. 2173-2176, 2020. [CrossRef] [Google Scholar] [Publisher Link]

[5] Chang-Jae Chun, Jae-Mo Kang, and Il-Min Kim, "Deep Learning-Based Joint Pilot Design and Channel Estimation for Multiuser MIMO Channels," *IEEE Communications Letters*, vol. 23, no. 11, pp. 1999-2003, 2019. [CrossRef] [Google Scholar] [Publisher Link]

[6] Liangtian Wan, Kaihui Liu, and Wei Zhang, "Deep Learning-Aided Off-Grid Channel Estimation for Millimeter Wave Cellular Systems," *IEEE Transactions on Wireless Communications*, vol. 21, no. 5, pp. 3333-3348, 2022. [CrossRef] [Google Scholar] [Publisher Link]

[7] Marius Arvinte, and Jonathan I. Tamir, "MIMO Channel Estimation Using Score-Based Generative Models," *IEEE Transactions on Wireless Communications*, vol. 22, no. 6, pp. 3698-3713, 2023. [CrossRef] [Google Scholar] [Publisher Link]

[8] Ahmet Emir et al., "Deep Learning Empowered Semi-Blind Joint Detection in Cooperative NOMA," *IEEE Access*, vol. 9, pp. 61832-61852, 2021. [CrossRef] [Google Scholar] [Publisher Link]

[9] Chi Nguyen, Tiep M. Hoang, and Adnan A. Cheema, "Channel Estimation Using CNN-LSTM in RIS-NOMA Assisted 6G Network," *IEEE Transactions on Machine Learning in Communications and Networking*, vol. 1, pp. 43-60, 2023. [CrossRef] [Google Scholar] [Publisher Link]

[10] Md. Habibur Rahman et al., "HyDNN: A Hybrid Deep Learning Framework Based Multiuser Uplink Channel Estimation and Signal Detection for NOMA-OFDM System," *IEEE Access*, vol. 11, pp. 66742-66755, 2023. [CrossRef] [Google Scholar] [Publisher Link]

[11] Xiaoyi Zhu et al., "A Deep Learning and Geospatial Data-Based Channel Estimation Technique for Hybrid Massive MIMO Systems," *IEEE Access*, vol. 9, pp. 145115-145132, 2021. [CrossRef] [Google Scholar] [Publisher Link]

[12] Y.G. Li et al., "MIMO-OFDM for Wireless Communications: Signal Detection with Enhanced Channel Estimation," *IEEE Transactions on Communications*, vol. 50, no. 9, pp. 1471-1477, 2002. [CrossRef] [Google Scholar] [Publisher Link]

[13] Yiqing Zhang et al., "Deep Expectation-Maximization for Joint MIMO Channel Estimation and Signal Detection," *IEEE Transactions on Signal Processing*, vol. 70, pp. 4483-4497, 2022. [CrossRef] [Google Scholar] [Publisher Link]

[14] Marcello Cicerone, Osvaldo Simeone, and Umberto Spagnolini, "Channel Estimation for MIMO-OFDM Systems by Modal Analysis/Filtering," *IEEE Transactions on Communications*, vol. 54, no. 11, pp. 2062-2074, 2006. [CrossRef] [Google Scholar] [Publisher Link]

[15] Muhammad Umer Zia et al., "Deep Learning for Parametric Channel Estimation in Massive MIMO Systems," *IEEE Transactions on Vehicular Technology*, vol. 72, no. 4, pp. 4157-4167, 2023. [CrossRef] [Google Scholar] [Publisher Link]

[16] Hui-Ping Yin et al., "Deep-Learning-Based Channel Estimation for Chaotic Wireless Communication," *IEEE Wireless Communications Letters*, vol. 13, no. 1, pp. 143-147, 2024. [CrossRef] [Google Scholar] [Publisher Link]

[17] Jae-Mo Kang, Chang-Jae Chun, and Il-Min Kim, "Deep Learning Based Channel Estimation for MIMO Systems with Received SNR Feedback," *IEEE Access*, vol. 8, pp. 121162-121181, 2020. [CrossRef] [Google Scholar] [Publisher Link]

[18] Aihua Zhang et al., "Channel Estimation for MmWave Massive MIMO with Hybrid Precoding Based on Log-Sum Sparse Constraints," *IEEE Transactions on Circuits and Systems II: Express Briefs*, vol. 68, no. 6, pp. 1882-1886, 2021. [CrossRef] [Google Scholar] [Publisher Link]

[19] In-Soo Kim, and Junil Choi, "FCFGS-CV-Based Channel Estimation for Wideband mmWave Massive MIMO Systems With Low-Resolution ADCs," *IEEE Wireless Communications Letters*, vol. 8, no. 6, pp. 1648-1652, 2019. [CrossRef] [Google Scholar] [Publisher Link]

[20] Rui Zhang et al., "Channel Estimation for mmWave Massive MIMO Systems with Mixed-ADC Architecture," *IEEE Open Journal of the Communications Society*, vol. 4, pp. 606-613, 2023. [CrossRef] [Google Scholar] [Publisher Link]

[21] Muneeb Ahmad, and Soo Young Shin, "Wavelet-Based Massive MIMO-NOMA with Advanced Channel Estimation and Detection Powered by Deep Learning," *Physical Communication*, vol. 61, 2023. [CrossRef] [Google Scholar] [Publisher Link]

[22] Zhen Chen et al., "Hybrid Evolutionary-Based Sparse Channel Estimation for IRS-Assisted mmWave MIMO Systems," *IEEE Transactions on Wireless Communications*, vol. 21, no. 3, pp. 1586-1601, 2022. [CrossRef] [Google Scholar] [Publisher Link]

[23] Hengtao He et al., "Deep Learning-Based Channel Estimation for Beamspace mmWave Massive MIMO Systems," *IEEE Wireless Communications Letters*, vol. 7, no. 5, pp. 852-855, 2018. [CrossRef] [Google Scholar] [Publisher Link]

[24] Asmaa Abdallah et al., "Deep Learning-Based Frequency-Selective Channel Estimation for Hybrid mmWave MIMO Systems," *IEEE Transactions on Wireless Communications*, vol. 21, no. 6, pp. 3804-3821, 2022. [CrossRef] [Google Scholar] [Publisher Link]

[25] Xisuo Ma et al., "Model-Driven Deep Learning Based Channel Estimation and Feedback for Millimeter-Wave Massive Hybrid MIMO Systems," *IEEE Journal on Selected Areas in Communications*, vol. 39, no. 8, pp. 2388-2406, 2021. [CrossRef] [Google Scholar] [Publisher Link]

[26] Iraj Naruei, and Farshid Keynia, "Wild Horse Optimizer: A New Meta-Heuristic Algorithm for Solving Engineering Optimization Problems," *Engineering with Computers*, vol. 38, pp. 3025-3056, 2022. [CrossRef] [Google Scholar] [Publisher Link]

[27] Shuai Cao et al., "A Novel Meta-Heuristic Algorithm for Numerical and Engineering Optimization Problems: Piranha Foraging Optimization Algorithm (PFOA)," *IEEE Access*, vol. 11, pp. 92505-92522, 2023. [CrossRef] [Google Scholar] [Publisher Link]

[28] B.M.R. Manasa et al., "A Novel Channel Estimation Framework in MIMO Using Serial Cascaded Multiscale Autoencoder and Attention LSTM with Hybrid Heuristic Algorithm," *Sensors*, vol. 23, no. 22, pp. 1-27, 2023. [CrossRef] [Google Scholar] [Publisher Link]

[29] Eva Trojovska, and Mohammad Dehghani, "Clouded Leopard Optimization: A New Nature-Inspired Optimization Algorithm," *IEEE Access*, vol. 10, pp. 102876-102906, 2022. [CrossRef] [Google Scholar] [Publisher Link]

[30] Muxuan Han et al., "Walrus Optimizer: A Novel Nature-Inspired Metaheuristic Algorithm," *Expert Systems with Applications*, vol. 239, 2024. [CrossRef] [Google Scholar] [Publisher Link]